

Electrosynthesis via Plasma Electrochemistry: Generalist Dynamical Model To Explain Hydrogen Production Induced by a Discharge over Water

Andressa Mota-Lima,^{*†} Jailton Ferreira do Nascimento,[‡] Osvaldo Chiavone-Filho,[§] and Claudio Augusto Oller Nascimento[†]

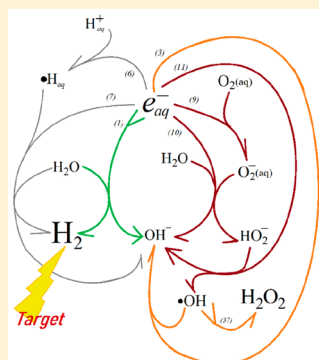
[†]Department of Chemical Engineering, Polytechnic School, University of São Paulo, USP, Avenue Prof. Luciano Gualberto 380, São Paulo, SP 05508-010, Brazil

[‡]CENPES, Research and Development Center, PDDP/TPP, PETROBRAS, Petróleo Brasileiro S.A., Avenue Horácio Macedo 950, Cidade Universitária, Ilha do Fundão, Rio de Janeiro, RJ 21941-915, Brazil

[§]Department of Chemical Engineering, Campus Universitário, Federal University of Rio Grande do Norte, UFRN, Lagoa Nova, Natal, RN 59078-970, Brazil

S Supporting Information

ABSTRACT: Electrosynthesis via electrochemical plasma, a discharge over the surface of liquid water (or plasma cathode), may offer an unprecedented route of synthesis for chemicals and (wind) solar fuels. Describing the physical chemical events underneath plasma/liquid interface (PLI) on a theoretical basis is crucial for enabling a rational designing of chemical synthesis. To address this problem, this work proposes a generalist dynamical model for the nanoreactor, a fraction of nanoliters localized beneath the PLI that features substantially high concentration of hydrated electrons (e_{aq}^-), and it screens chemical reaction networks (CRN) related to the synthesis of hydrogen, a model electrosynthesis process. The computational results elucidate two major routes for hydrogen production: (a) in very alkaline media, the water reduction via self-recombination of e_{aq}^- [$2e_{aq}^- + 2H_2O \rightarrow H_2 + 2OH^-$] consumes the majority of e_{aq}^- , whereas (b) in very acid media, e_{aq}^- is majorly scavenger by the ion H_{aq}^+ , generating an abnormally high concentration of the radical H^\bullet , a precursor for gaseous hydrogen. Additionally, two scenarios are disadvantageous for synthesizing H_2 . Side reactions with aqueous oxygen and aqueous radical $\cdot OH$ leads to substantial production of O_2^- and OH^- , respectively. Without loss of generality, the dynamical model proposed in this work is a powerful theoretical frame for understanding and predicting a variety of plasma-induced CRNs, assisting to advance the emerging field of plasma electrochemistry.



1. INTRODUCTION

Since this topic has been studied, the potential of chemical synthesis based on a cold plasma has been based on repeated reports about hydrogen production for the discharges either over¹ or in^{2–4} liquid water, with such configuration termed herein as electrochemical plasma. This is mainly because both the plasma and the water connect along a single conductive path between the two metallic terminals of the high-voltage power supply, so the plasma itself acts as an electrochemical cathode. If it were otherwise, where the plasma was the sole conductor in between the two metallic terminals, gas injection (jet effect) is required to spread the discharge over the liquid, promoting the discharge/liquid contact that is termed the plasma/liquid interface (PLI), and such a configuration is called torch-like plasma. Both the electrochemical plasma and the torch-like plasma are able to synthesize chemicals, however in different phases (see Glossary in the Supporting Information for detailed definitions on those configurations). The plasma effluent in contact with water enriches the liquid phase with a variety of radicals,^{5–8} and despite inducing both oxidation^{2,9,10}

and radical initiator reactions¹¹ in the liquid phase, hydrogen production for a torch-like configuration develops in the plasma phase, as result of either the reforming reaction of hydrocarbon^{12–19} or the splitting of water.^{4,20–26} Contrariwise, hydrogen production steered by an electrochemical discharge is mostly developed in the liquid phase. To elucidating the major facts, the literature noted in this Introduction directs the reader to the theoretical frame hereby proposed, instead of offering an extensive review.

More recently, the successful reduction of aqueous carbon dioxide to oxalic plus formic acid²⁷ by an electrochemical discharge renewed the belief in such an electrosynthesis via electrochemical plasma. It is largely known that a variety of electrochemical discharges (glow discharge in and over water, jet discharge over water, etc.), or *plasma electrolysis* as named by the plasma community, are able to reduce a broad spectrum

Received: May 20, 2019

Revised: August 8, 2019

Published: August 12, 2019

of aqueous cations such as Cu^+ and Pt^+ to mention a few.²⁸ In recent years, reduction of cations such as Ag^+ ^{29,30} and Au^+ ^{31–35} was systematically employed to mimetically gain information on the mechanism of reduction-like reactions due to the plasma–liquid interaction. Despite all experimental efforts, the lack of a theoretical frame about the physical chemical events within the liquid phase directed by the plasma–liquid interaction greatly limits our ability to make rational design on the chemical routes. Aiming at clarifying possible ways of designing routes for chemical synthesis, this work proposes a dynamical model for a confined region in the liquid, describing the physical chemical events in it. The mechanism of hydrogen production is unveiled along with the task of understanding the chemical route related to its synthesis. To this end, the synthesis of hydrogen acts as a model process for plasma-based electrosynthesis steered by an electrochemical discharge.

Figure 1 outlines the PLI, emphasizing the spatial position of the reactor termed nanoreactor because its volume has a

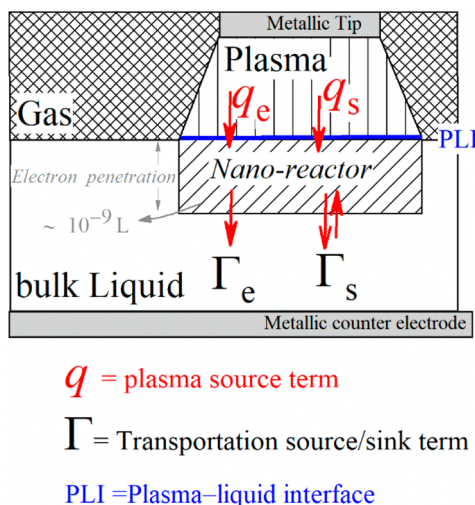


Figure 1. Out of proportion sketch of the electrochemical nanoreactor generated during an electrochemical discharge.

fraction of 10^{-9} L when pondering differences in the time scales for both chemical and diffusion events³⁶ related to the hydrated electrons (e_{aq}^-). The electrosynthesis develops mostly within such nanoreactor. An uncontested proof of a substantially high concentration of e_{aq}^- spatially confined in a region that this work terms nanoreactor was recently accomplished using a spectroscopic method.³⁷ This finding settles e_{aq}^- as the first and most important reactant within the nanoreactor. The identification of other essential reactants (essential chemical variables) in the context of plasma-driven reactions is determined by whether their concentrations are near the order of magnitude for the e_{aq}^- concentration. An inspection of the radiolysis-based reactions aids to identify other possible reactants whose classification is found in the second section of this work, **Theory**.

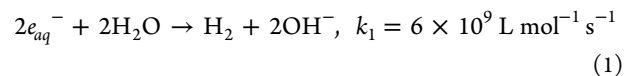
This work makes ample use of the chemical reaction networks (CRN) to propose *chemical dynamic models*. This is mainly because the electrosynthesis via electrochemical plasma develops under a periodic perturbation on the e_{aq}^- concentration within the nanoreactor. If it were otherwise, key information would be lost by analyzing the rate law of reactions individually or by evaluating the pre-exponential rate

constants comparatively. Advantageously, CRN-based models deal with the full set of reactions all at once, treating the chemical mechanism as a dynamical system.^{38–40} This work engages in a screening of CRNs by assembling elementary reactions from the radiation chemistry of water.⁴¹ Each experimental scenario of discharge forges its own CRN. The chemical mechanisms are conveniently represented in so-called network diagram (or set-graph diagrams)³⁸ in which the species symbols are connected by arrows according to the stoichiometric constraints imposed by each reaction. In a network diagram, the number of barbs on an arrow pointing to a product indicates the stoichiometric coefficient of this product in the respective reaction, while the number of left feathers indicates the stoichiometric exponent of the reactant. By convention, no feathers are shown when the stoichiometric and kinetic coefficient of a reactant are both unity. Accurately, the graph diagrams without cycles (autocatalytic reactions) are called trees, which differentiate by means of the nomenclature the stability of the network; i.e., the dynamic system associated with the trees allows only for steady stationary states. The plasma-induced CRNs-trees are stable networks despite being driven by a periodical perturbation on the e_{aq}^- concentration.

This work unravels CRNs for two major scenarios. The first one considers a discharge in noble gas over water enriched with either acid, salt or hydroxide, revealing the core CRN related to the hydrogen synthesis, cf. section 3.1. The second major scenario depicts the drawbacks for hydrogen synthesis in the presence of species acting like scavengers of e_{aq}^- . For example, the plasma-synthesized species such as nitrate (produced via the Birkeland–Eyde process by discharge over mixture of N_2 and O_2 gases) and radical $\cdot\text{OH}$ (produced by discharge over humid gas) are treated in sections 3.1.3 and 3.2, respectively, together with the soluble gases (oxygen) treated in sections 3.3. All the scenarios studied herein employ the electrical data found in the work of Urabe et al.⁴² that was employed as a model standard for a pulsed DC-voltage.

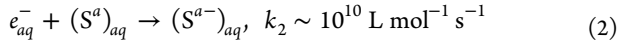
2. THEORY

2.1. Radiolysis-Based Reactions Steered by Electrochemical Plasma. In this section, all radiolysis-related reactions involved with e_{aq}^- are gathered. Gonzalez et al.³⁶ overestimates that the instantaneous e_{aq}^- concentration is about 0.6 mol L^{-1} within a time scale as narrow as 1 ns (10^{-9} s) when considering the volume of some 10^{-9} L. Such a considerable concentration sets e_{aq}^- as the first and most important reactant, leading to a substantial production of gaseous hydrogen



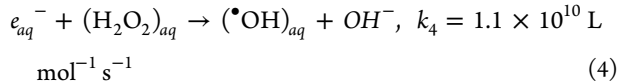
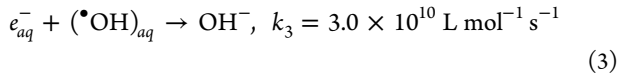
in connection to a local production of OH^- . Reaction 1 is also known as second order recombination reaction. Over time, it leads to the basification of the liquid body. A strong signal of validation on this path is observed in the findings of Witzke et al.¹ that had detected gaseous hydrogen into the gaseous plasma effluents, via mass spectroscopy, while simultaneously observing a global rise on the pH of the liquid body. An incontestable final validation, however, for this pathway termed herein as *via–Self-recombination*, or *via–Self* for short, would be accomplished by simultaneously quantifying the stoichiometry between moles of H_2 , OH^- , and e_{aq}^- . This will be the direction exploited throughout this work. If the hydrogen

production follows strictly reaction 1, the moles of H₂, OH⁻, and e_{aq}⁻ have to follow a ratio 1:2:2. All other pathways competes with the *via-Self* for e_{aq}⁻ because the hydrated electron reduces a scavenger (S) species, also in liquid phase, via the *scavenger-like reaction*, or *via-S*

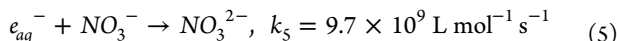


Several aqueous ions/species take over the scavenger role. This work targets three major classes of scavengers that relate to (a) the plasma-synthesized species; (b) the supporting electrolyte, a chemical substance whose function is to increase the ionic conduction of the liquid electrolyte; and (c) the dissolvable gases in aqueous phase.

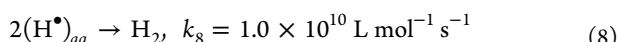
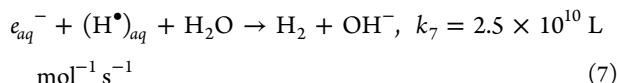
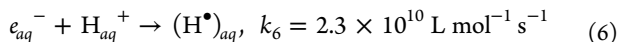
Among the scavengers related to the plasma-synthesized species are hydronium radical (•H), hydroxyl radical (•OH), H₂O₂, NO₃⁻, and NO₂⁻. The former three must be considered for a humid-based discharge, whereas the latter two are observed for an air-based discharge. Radical species are produced in the plasma phase and invariably uptaken by the liquid phase,⁵ thus making their presence in the nanoreactor unavoidable. This work targets specifically the humid-plasma-induced species such as •OH radical and H₂O₂ that consume e_{aq}⁻ while producing OH⁻



which could not only decreases the yields of hydrogen production but also modifies the stoichiometric proportion between the global molar production of OH⁻ and H₂. Additionally, the nitrate synthesized via the well-known Birkeland–Eyde process⁴³ for an air-based discharge is also considered as a possible scenario. Even if not intentionally added to the bulk liquid as HNO₃, nitrate could be uptaken by the liquid from the plasma/gas phase as reported elsewhere.⁴⁴ The nitrate is reduced by e_{aq}⁻ via

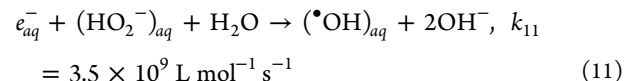
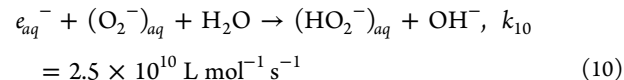
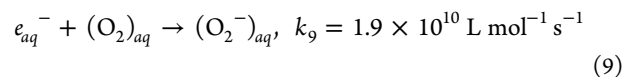


From this point on, the scavengers related to the supporting electrolyte are treated. This work deals solely with the hydronium ion (H⁺) because it is invariably present in pure water. The hydronium ions provide an additional route for H₂ production based on a two-steps mechanism⁴⁵



Finally, to complete the description for the mechanism involving e_{aq}⁻ as reactant in the nanoreactor, the scavengers related to dissolvable gases are hereby considered. The water body is a great reservoir for gases like O₂ and CO₂ that under SPT conditions are in concentrations around 270.0 and 13.6 × 10⁻⁶ mol L⁻¹, respectively. Such values of scavenger concentration must not be disregarded. For simplicity, only

one gas-based scavenger is considered, the dissolved oxygen, which introduces the following cascade of pathways



2.2. Defining Physical Boundaries, Transportation Rates (Γ) in the Liquid Phase and Rates for both Chemical (q_S) and Electrical (q_e) Interactions at PLI. The first and most important physical boundary for modeling the plasma-induced reactions in liquid phase is the definition of the reactor volume, a crucial parameter for defining the local concentration of the reactants. Assuming the full volume of the liquid body as a reactor is unrealistic because the discharge over the liquid is a localized event, meaning that the chemical events relaxes at shorter time scale than does the transportation events. Defining the conceptual boundaries of the reactor is a vital task. The contact area of the PLI is around a thousand times smaller than the area of gas/liquid contact (for more details, see Table S2). The primary plasma-based reactant, the e_{aq}⁻, penetrates only a few nanometers³⁷ into the liquid phase. Pondering all of this, the volume related to the nanoreactor rarely exceeds some 10⁻⁹ L.

Figure 1 depicts both the relative position between the two metallic terminals with respect to the water surface and, by arrows, the flows of species through the boundaries of the nanoreactor as result of either transport events in liquid phase (term Γ) or plasma-liquid interaction (term q). The plasma phase takes over the role of working electrode (WE) whereas the counterpart metallic terminal acts as the counter electrode (CE). In the configuration depicted in Figure 1, a net current of charge flows through the plasma and liquid phase with the same magnitude, which is a prerequisite to classify the cold plasma as electrochemical and a fundamental differing it from the torch-like configuration. No electrical constriction exists for a PLI generated by a torch-like plasma, being the interaction plasma/liquid ordinarily governed by Henry's law. Conversely, an electrified PLI sets very clear boundary conditions for the electrical charge transportation through the PLI, the PLI is an electrical element subordinated to the Kirchhoff's current law. Such condition allows to connect the electrical current (J), gauged somewhere in the electrical section between the power supply and the plasma, to the electrical current flowing throughout the PLI. For a cathodic discharge, the division of J by Faraday's constant yields the rate of ballistic electrons (Δn_e) that are injected into the nanoreactor per unit of time (Δt). The term q_e is defined as the release rate of ballistic electrons into the nanoreactor

$$q_e \equiv \frac{\Delta n_e}{\Delta t} = \frac{J}{96485} \quad (12)$$

The ballistic electrons transform into hydrated electrons after injection, increasing instantaneously the local concentration of e_{aq}⁻, i.e., the concentration inside the nanoreactor. The action of a localized increase on the concentration creates a gradient of concentration between the nanoreactor and the bulk liquid,

Table 1. Parameters Employed To Solve, via the Interactive Method, Equations 14 and 15 across Different CRNs

parameter		value	unit
release rate of ballistic electrons	q_e^a	$1,555.0 \times 10^{-9}$	mol s^{-1}
	$\frac{1}{V} \times q_e$	$659.00 \times 10^{\circ}$	$\text{mol L}^{-1} \text{s}^{-1}$
release rate of the Birkeland–Eyde products	$q_{\text{NO}_3} = q_{\text{H}^+}^b$	293.34×10^{-12}	mol s^{-1}
	$\frac{1}{V} \times q_{\text{NO}_3} = \frac{1}{V} \times q_{\text{H}^+}$	12.43×10^{-2}	$\text{mol L}^{-1} \text{s}^{-1}$
release rate of radical OH (torch-like interaction)	$\frac{1}{V} \times q_{\text{OH}}^c$	25.39×10^{-6}	$\text{mol L}^{-1} \text{s}^{-1}$
release rate of hydrogen peroxide (anodic plasma/electrochemical discharge)	q_{OH}^e	$20,000.0 \times 10^{-9}$	mol s^{-1}
	$\frac{1}{V} \times q_{\text{OH}}^e$	$8,470.00 \times 10^{\circ}$	$\text{mol L}^{-1} \text{s}^{-1}$
volume of the nanoreactor ^b	V	2.36×10^{-9}	L (at STP)
rate coefficients	k_1^d	6.0×10^9	$\text{L mol}^{-1} \text{s}^{-1}$
	k_2^d	1.1×10^{10}	
	k_3^d	3.0×10^{10}	
	k_4^d	1.1×10^{10}	
	k_5^d	9.7×10^9	
	k_6^d	2.3×10^{10}	
	k_7^d	2.5×10^{10}	
	k_8^d	1.0×10^{10}	
	k_9^d	1.9×10^{10}	
	k_{10}^d	2.5×10^{10}	
	k_{11}^d	3.5×10^9	
	k_{37}^d	5.0×10^9	
	k_{38}^d	2.5×10^{10}	
initial concentrations for the scavengers at the time zero	$[\text{H}^+]_0 / \text{pH} = 1$	1.0×10^{-1}	mol L^{-1}
	$[\text{H}^+]_0 / \text{pH} = 7$	1.0×10^{-7}	
	$[\text{H}^+]_0 / \text{pH} = 8$	1.0×10^{-8}	
	$[\text{H}_2\text{O}_2]_0^c$	5.0×10^{-8}	
	$[(\text{O}_2)_{\text{aq}}]_0$ at 0.20 atm^f	2.7×10^{-4}	
	$[(\text{O}_2)_{\text{aq}}]_0$ at 0.0005 atm^f	6.5×10^{-7}	
	$[(\text{O}_2)_{\text{aq}}]_0$ at 0.10^{-10} atm^f	1×10^{-12}	

^aEstimated by this work based on the discharge extracted from the work of Urabe et al.,⁴² see Table S1. ^bThe largest acidification rate observed on the data from the work of Gonçalves et al.³⁰ ^cReal concentration expect for the time window of the DC-pulse estimated from the data found on the work of Gorbanov et al.⁵ ^dIn general, the rate constant for all the reactions were gathered from Garrett et al.⁴¹ and Buxton et al.⁴⁷ ^eEstimated from Liu et al.⁴⁶ ^fMolar solubility of oxygen in water at the sea level (1 atm) estimated by using the Henry law constants for oxygen in water at 298 K and considering different partial pressures.

driving two major processes in the liquid phase: the chemical reactions and the transportation. The chemical phenomenon is captured by the function f_{CRN} that will be discussed below, and the transportation of e_{aq}^- toward the bulk liquid develops via action of concentration gradient (diffusion) and electrical gradient (electrical drift). The term Γ_e encompasses all the natures of e_{aq}^- transportation. The arrows in Figure 1 for the term Γ_e assumes a single direction because the concentration of e_{aq}^- is invariably always larger at the nanoreactor than at the bulk liquid. By convention, the flow of species departing from the nanoreactor toward the bulk liquid has a negative signal.

Only a scavenger having a high solubility into the aqueous liquid will attain a concentration reasonably near to the concentration of e_{aq}^- . The water is in abundance; therefore its concentration as reactant will be disregarded completely. If the scavenger is already part of the liquid, its initial concentration in the nanoreactor will be considered equal to the concentration of the bulk liquid. If otherwise, it will be zero as was the case for plasma-induced scavenger, for instance nitrate and radical OH. Additionally, the injection rate of plasma-induced scavenger into the nanoreactor is driven by the plasma-induced source term, or q_s , that quantifies the positive variation on the moles of plasma-induced scavenger (Δn_s) into the nanoreactor per unit of time (Δt)

$$q_s \equiv \frac{\Delta n_s}{\Delta t} \quad (13)$$

The value of the plasma-induced scavenger source, q_s , is highly dependent on the parameters (gas composition and flow) and nature (glow discharge, DBD etc.) of the plasma source. In this work, plasma-induced scavenger source q_s is solved for three scavengers, the radical $\cdot\text{OH}$ (q_{OH}) plus the Birkeland–Eyde products that includes both H^+ (q_{H^+}) and NO_3^- (q_{NO_3}), as listed in Table 1. After uptake by the liquid, these scavengers increase their local concentration and suffer both chemical reactions and transportation toward bulk liquid. The term Γ_s in Figure 1 accounts for such transportation of scavenger. In general, the scavenger transportation has a positive sign because the species departs from outside to inside the nanoreactor. The bulk liquid is the sources of scavenger related to both the supporting electrolyte and the aqueous gases, once it has high concentration of these scavengers. Exceptionally for scavengers synthesized in plasma phase (radical $\cdot\text{OH}$ for instance), a negative sign for the term Γ_s could be set, once the concentration gradient has an inverted direction.

2.3. The Generalist Dynamical System. A generic dynamic model to describe the temporal evolution for the

concentration of both e_{aq}^- , $[e^-]$, and scavenger, $[S]$, in the nanoreactor during a discharger is described respectively by

$$\frac{d[e_{aq}^-]}{dt} = -f_{CRN} + \frac{1}{V}q_e - \Gamma_e \quad (14)$$

$$\frac{d[S]}{dt} = -f_{CRN} + \frac{1}{V}q_s \pm \Gamma_s \quad (15)$$

where the variation q_e in eq 14 stands for the release rate of ballistic electrons per discharge that is essentially defined by the level of the current as already discussed in section 2.2; the variation q_s in eq 15 stands for the uptake rate of the plasma-induced scavenger by the liquid. Both q_e and q_s are continuous functions representing source term in the differential eqs 14 and 15, a plasma-induced term that is either zero or positive. V is the volume of the nanoreactor at the discharge onset, and its variation during the discharge period (t_p) is assumed to be neglectful. Last, the terms Γ_e and Γ_s stand for the rate of transportation of the main chemical reactants into/from the nanoreactor. In this work, no transport event is considered, whether diffusion or convection, thus leading to zero values for both Γ_s and Γ_e .

The function f_{CRN} encompasses the kinetic mechanism described by each CRN-tree. Each independent chemical variable in the eqs 14 and 15 counts contributions from several pathways (i) contained in the CRN

$$f_{CRN} = \sum_i k_i \prod_j [R_j]^{\kappa_{ij}} \quad (16)$$

where the $[R_j]$ is the concentration of the j th reactant, k_i is the coefficient rate for the i th reaction, and κ_{ij} stands for the stoichiometric coefficient for the reactant R_j in the i th reaction. Each pathway contributes with one term known as the rate of reaction (v_i),

$$v_i = k_i \prod_j [R_j]^{\kappa_{ij}} \quad (17)$$

that is embedded into eq 16. The rate of reaction, v_i , express the law of mass action.

In the eqs 14 and 15, the following independent variables are function of time

$$[S^+] = f(t) \text{ and } [e_{aq}^-] = f(t)$$

Equations 14 and 15 represent a generalist chemical dynamic model based on CNR tailored under realistic boundary conditions. To access the temporal evolution of the independent variables, eq 14 and 15 are solved as linear system of ordinary differential equations via the interactive method carried out with Wolfram language (Wolfram Mathematica). Table 1 displays the values of all parameters employed in the numerical solution. The source term q_s was estimated from several papers,^{5,36,46} and all the rate coefficients were extract from elsewhere.^{41,47} The electrical data from Urabe et al.⁴² enable us to access a crucial parameter for the kinetic model, the release rate of ballistic electrons (the term q_e). Furthermore, the global yields of the main products are computed by

$$\frac{d[P]}{dt} = f_{CRN}^p \quad (18)$$

The differential equation eq 18 refers to the time evolution for the concentration of a given product, called P. Among the

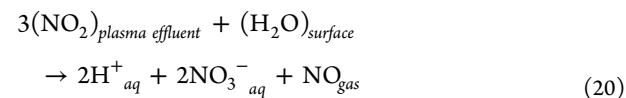
main products, P, of a given CRN are the gaseous hydrogen (H_2), OH^- ions, and reduced scavenger (S^{a-}), meaning that P = { H_2 , OH^- and S^{a-} }. The continuous function f_{CRN}^p describes the temporal evolution of the concentration of productions

$$f_{CRN}^p = \sum_i \frac{\kappa_{ij}}{\kappa_{ip}} v_i \quad (19)$$

within the i th balanced reaction in the CRN-tree. Differential eq 18 is defined as a dependent variable because it is a linear combination of the chemical variables assigned to the reactants, the independent variables. Equation 19 is a continuous function that connects the rate of formation of products to the rate of consumption of reactants (eq 17) by multiplying eq 17 by the stoichiometric coefficient of the j th reactant (κ_{ij}) and simultaneously dividing it by the stoichiometric coefficient of the product (κ_{ip}) within the i th balanced reaction in the CRN-tree.

3. RESULTS

3.1. Dry Discharge over Oxygen-Free Electrolyte. This section is subdivided into three sections to understand the CRNs when the discharge over liquid occurs in dry gas phases and in a complete absence of oxygen solubilized into aqueous phase. Such experimental condition imposes clear consequences to solve the model in eq 14–15. First, there is no gas-phase source of scavenger, such as soluble oxygen. Second, the absence of water vapor in the plasma phase suppresses from our analysis both H_2O_2 and radicals $\cdot OH$ because of their negligible concentration relates to a neglectful mass action of their scavenger-like behavior. Third, two cases related to the plasma-synthesized species are considered: the air-based and the air-free plasma phase. For air-based plasma, the Birkeland–Eyde process of nitrogen fixation⁴³ produces the plasma-phase nitrite (NO_3^-) that dissolves into the liquid body by means of the chemical interaction in the surface between water and the plasma-effluents



Reaction 20 is associated with other fluid dynamic processes developed for a discharge with jet effect.⁴⁸ The air-based discharge imposes over the model 14–15 clear constraints: (a) two nonzero plasma-induced sources of scavenger, i.e., $q_s \rightarrow q_H$ and $q_s \rightarrow q_{NO_3}$ where $q_H > 0$ and $q_{NO_3} > 0$; and (b) the presence of at least two scavengers, the hydronium cation and the nitrite anion, S = { H^+ and NO_3^- }. Contrariwise, the air-free plasma invalidates these conditions. Finally, three supporting electrolytes are tested: HCl, NaCl, and NaOH. On doing so, the water pH moves respectively from acid to neutral to basic, which manipulates the concentration of the hydronium ion, a scavenger based on the electrolyte.

3.1.1. Air-Free Discharge over either Neutral (NaCl) or Acid (HCl) Aqueous Electrolyte. In air-free dry discharge, the unique class of scavenger present in the nanoreactor is the supporting electrolyte, and this section analyses two of them: HCl and NaCl. Either Cl^- or Na^+ are inert as the scavenger but the hydronium cation (H^+) does activate the pathway through reactions 6–8. These reactions include the radical H^\bullet as an intermediate species; see the CNR-tree in Figure 2. Such CRN-tree assembles reaction 1 plus reactions 6–8, and the

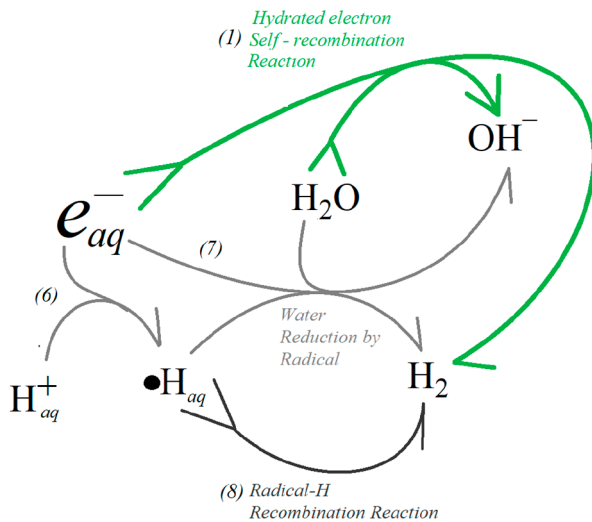


Figure 2. CRN-tree (or mechanism) for an air-free dry discharge over water containing either HCl or NaCl as supporting electrolyte.

associated dynamical system is depicted by the temporal evolution of the reactants, which is accessed by

$$\frac{d[e_{aq}^-]}{dt} = -\{2k_1[e_{aq}^-]^2 + k_6[H^+][e_{aq}^-] + k_7[\cdot H][e_{aq}^-]\} + \frac{1}{V}q_e \quad (21)$$

$$\frac{d[H^+]}{dt} = -k_6[H^+][e_{aq}^-] \quad (22)$$

However, the intermediate species (radical H[•]) is depicted by

$$\frac{d[\cdot H]}{dt} = k_6[H^+][e_{aq}^-] - \{2k_8[\cdot H]^2 + k_7[\cdot H][e_{aq}^-]\} \quad (23)$$

The chemical dynamical system encompassed by eqs 21–23, when solved, allows us to access the temporal evolution for the products by

$$\frac{d[H_2]}{dt} = k_8[\cdot H]^2 + k_1[e_{aq}^-]^2 + k_7[\cdot H][e_{aq}^-] \quad (24)$$

$$\frac{d[OH^-]}{dt} = 2k_1[e_{aq}^-]^2 + k_7[\cdot H][e_{aq}^-] \quad (25)$$

Note that, in the CRN-tree from Figure 2, there are four species among reactants and intermediates, but only three are independent variables on the dynamical model in eqs 21–23. Each one of these equations describes the temporal evolution of the concentrations of e_{aq}^- , H^+ , and $\cdot H$. The water acting as reactant in reaction 1 is in abundance, and its concentration does not vary over time into the nanoreactor; thus, this reactant is disregarded as a chemical variable. Note also that the temporal evolution of the final products, accessed via eqs 24 and 25, depends solely on two independent variables, the concentration of e_{aq}^- and H^+ . Such comments implicate that (a) eqs 21–23 are solved as linear system of differential equations via numerical methods and (b) the temporal solutions for these three independent variables (concentrations of e_{aq}^- , H^+ , and $\cdot H$) were employed to solve eqs 24 and 25, the dependent equations. Figure 3 shows temporal solutions obtained by this procedure. The concentrations in either Figure 3 or any other similar figure is, indeed, variations of concentration within the incremental step (10^{-6} second, in this work) employed in the numerical method. Instead of molarity, this work also considers the yields of products, defined as the final moles of products obtained at the ending time of discharge. For this reason, the temporal evolution of products obtained with eqs 24 and 25 are integrated over a full period of discharge that is either 0.1 or 0.2 ms and then multiplied by V. Figure 5 displays the final moles of products obtained by this integration procedure.

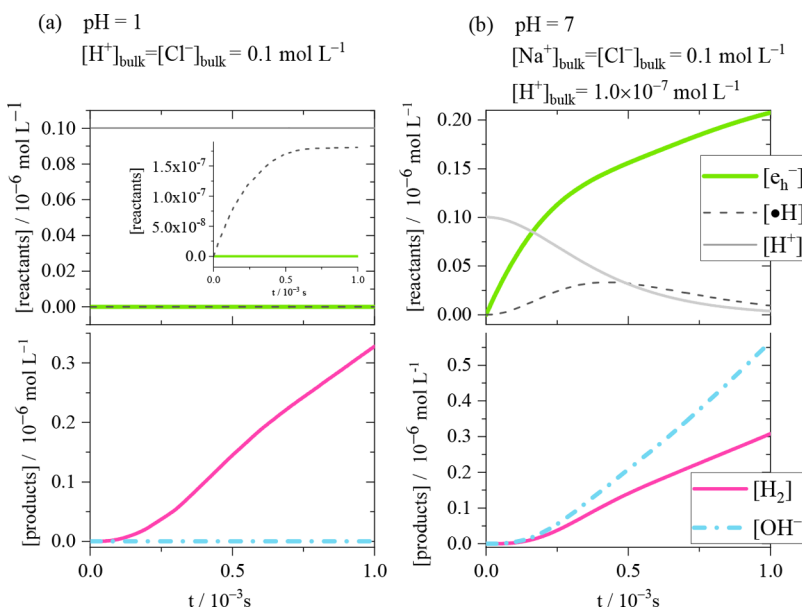


Figure 3. Temporal evolution of reactants and products accessed by computational experiments solving eqs 21–23 as independent variables of the dynamical system and considering two initial concentrations of hydronium (a) $[H^+]_0 = 10^{-1} \text{ mol L}^{-1}$ and (b) $[H^+]_0 = 10^{-7} \text{ mol L}^{-1}$. Initial condition: $[e_{aq}^-]_0 = [\cdot H]_0 = 10^{-17} \text{ M}$ whereas $[H^+]_0 = [H^+]_{\text{bulk}}$. The values for all other parameters are listed in Table 1.

The concentration of hydronium ion is manipulated by the electrolyte pH. For 0.1 mol L^{-1} HCl, the electrolyte pH settles around 1 and $[\text{H}^+]$ equals 0.1 mol L^{-1} . On the other hand, pH around 7 is obtained with 0.1 mol L^{-1} NaCl, and $[\text{H}^+]$ equals $10^{-7} \text{ mol L}^{-1}$. In principle, the aqueous NaCl solution must have pH around 7, but in reality, it has lower pH due to the CO_2 dissolution. However, the experiments in this work are computational; thus, considering pH = 7 for aqueous NaCl solutions is fairly appropriate.

The concentration of hydronium ion demonstrated a profound impact on the preferential routes for hydrogen production. Figure 3 displays the time evolution for the concentration of reactant and products for pH 1 and 7, which are respectively a high and low concentration of hydronium ion. Hydrogen is produced for both pHs, however OH^- is produced only in neutral pH. Such difference on the distribution of products is consistently explained based on the mechanism shown in Figure 2. For high concentration of H^+ , the formation of radical-H (H^\bullet) via reaction 6 has a substantially high rate, speeding up all reactions downward. The near zero production of OH^- in Figure 3 for pH 1 indicates the water reduction either via hydrated electron self-recombination (reaction 1) or via assistance by radical-H (reaction 7) are irrelevant routes, so hydrogen is fully produced via a radical-H recombination reaction (reaction 8). Furthermore, this interpretation corroborates with the time evolution of reactants for pH 1, cf. Figure 3a. Neither the concentration of H^+ decreases, nor does the concentration of e_{aq}^- rise above zero, but the concentration of radical $\cdot\text{H}$ rises smoothly, going from zero to $1.5 \times 10^{-7} \text{ mol L}^{-1}$. Indeed, the concentration of radical H^\bullet remains low, despite a fast hydronium scavenger reaction rate (reaction 6), because of its fast recombination rate via reaction 8, that drags H^\bullet out into the substantial formation of gaseous hydrogen as seen on the bottom plate (a). Additionally, the concentration of e_{aq}^- fixed around zero is consistent with negligible rates for both reactions 1 and 7. As a partial conclusion, the radical-H recombination reaction is the major route for hydrogen production in highly acid pH.

Considering the low concentration of H^+ in Figure 3 (pH 7), the time evolution of concentrations of both reactants and products indicate a change on the preferential route of H_2 production, as discussed below. A stiff increase in the OH^- concentrations seen in plate b revels that both reactions 1 and 6 have a nonzero rate, which is corroborated by a nonzero concentration of both e_{aq}^- and $\cdot\text{H}$. Furthermore, the maximum on the profile for the $\cdot\text{H}$ (an intermediate species) associated with a monotonic depletion on the H^+ concentration indicates that the rate of either reaction 6, 7, or 8 is being reduced progressively. As a final piece in this dynamical evolution, the rate of reaction 1 develops an uninterrupted rise in Figure 3b because of the progressive increase on the e_{aq}^- concentration. This view gains precision with a computational assessment of the rates of reaction shown in Figure 4. The rate of reaction 1 overpasses all the others over the majority of the discharging time, therefore indicating that the self-recombination of hydrated electron (reaction 1) is the dominant route of hydrogen production in neutral media. In addition, the H^\bullet is an active intermediate that generates hydrogen via reaction 7, with this route being the second and last relevant pathway in neutral media. To conclude, the hydrogen generated in neutral media is in a major way explained by the self-recombination of

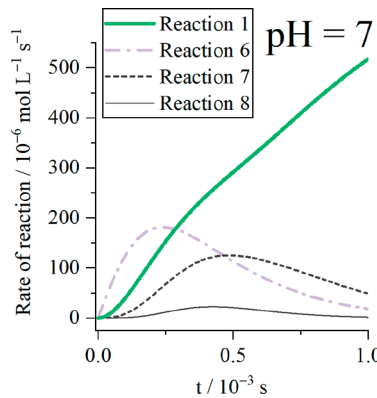
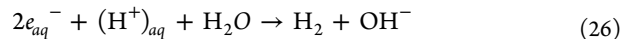


Figure 4. Rate of reactions for all the steps in the CNR from Figure 2 accessed by computational experiments solving eqs 21–23. Initial condition: $[e_{aq}^-]_0 = [\cdot\text{H}]_0 = 10^{-17} \text{ M}$ whereas $[\text{H}^+]_0 = [\text{H}^+]_{\text{bulk}} = 10^{-7} \text{ mol L}^{-1}$. The values for all other parameters are listed in Table 1.

e_{aq}^- (reaction 1) and just in a minor way by the radical-H assisted water reduction (reaction 7).

Such perception of the dominance of one pathway over another in a real life experimental is captured by quantifying the stoichiometric proportion between products together with the stoichiometric quantity of ballistic electrons. Table 2 summarizes the stoichiometric ratio $\text{H}_2:\text{OH}^-:e_b$ for the three dominating routes of hydrogen production according to the pH. The stoichiometric proportion must adhere to one of the extreme cases, either pH 1 or pH 7 seen in Figure 5 or, otherwise, lay in between them for intermediate pHs. In addition to the yields of products and the influx of ballistic electron, Figure 5 stresses the stoichiometric ratio between those quantities. On one extreme, at pH 1, each mole of hydrogen relates to zero mole of OH^- and around two moles of ballistic electrons, i.e., a ratio $1:0:\geq 2$. On the other extreme, the pH 7 displays a ratio $1:\leq 2:\geq 2$. In principle, the expected ratio in acid media is $1:0:2$ whereas for neutral media $1:\leq 2:2$. If compared to Table 2, the ballistic electron ratio deviates upward of 2, which indicates that not all ballistic electrons had reacted in the liquid phase under the time span considered in the particular case of Figure 5. When accounting for the yields under full period of discharge, i.e., during 0.2 ms of both closed and open sections, the deviation smooths as shown in Figure 6. In an abundance of H^+ ions as for pH 1, the radical-H is an active intermediate and the stoichiometric ratio H_2 to OH^- follows 1:0 straightforwardly. Conversely, in a scarcity of H^+ ions, as for pH 7, radical-H continues to be an active intermediate but with a rather low contribution to the total yield of hydrogen. In addition, the preferential pathway for synthesis of H_2 via radical-H is seen to be the radical-assisted water reduction that includes the 6 plus reaction 7 combined into a global reaction



for which the ratio of H_2 to OH^- follows 1:1. In neutral media, the self-recombination of e_{aq}^- is the major pathway contributing to the total yield of hydrogen; thus the global observation carries the general tendency for its ratio H_2 to OH^- of 1:2. The contribution of the radical-assisted water reduction to the total amount of produced hydrogen, despite being minor, fairly deviates the ratio H_2 to OH^- toward $1:\leq 2$. The direction of deviation can not only be understood but also

Table 2. Stoichiometry Proportion between Several Pathways for Hydrogen Production via Electrochemical Plasma

routes of hydrogen production	via	domain range	ratio H ₂ :OH ⁻ :e _b
reaction 1: 2e _{aq} ⁻ + 2H ₂ O → H ₂ + 2OH ⁻	self	pH ≥ 7	1:2:2
reactions 6 + 7: 2e _{aq} ⁻ + (H ⁺) _{aq} + H ₂ O → H ₂ + OH ⁻	radical-H assisted water reduction	1 < pH < 7	1:1:2
reactions 6 + 8: 2e _{aq} ⁻ + 2(H ⁺) _{aq} → H ₂	radical-H recombination	pH ≤ 1	1:0:2

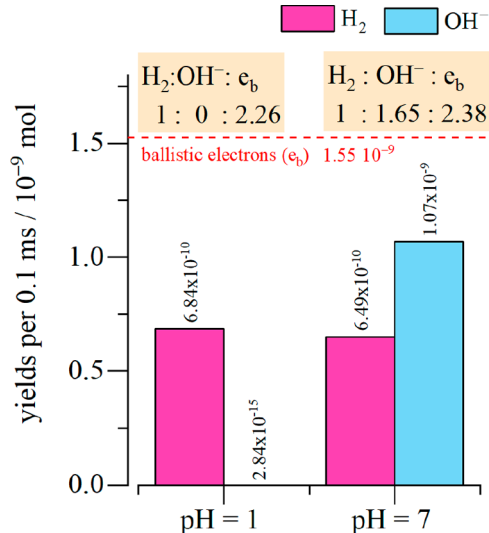


Figure 5. Yields of gaseous hydrogen and aqueous OH⁻ when solving eqs 21–23 by computational experiments for the period of closed section, i.e., 0.1 ms. The red dashed line represents the total amount of ballistic electrons (e_b) converted into hydrated electrons per discharge.

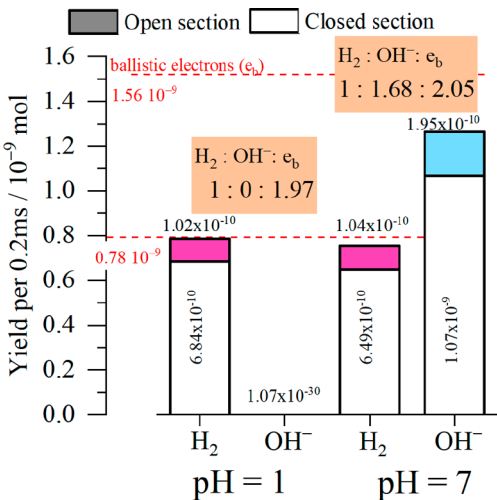


Figure 6. Bar graph for yields of gaseous hydrogen and aqueous OH⁻ when considering the period of closed section plus the open circuit period of a pulsed DC-voltage discharge (total of 0.2 ms) when solving eqs 21–23. The red dashed lines represent the values of ballistic electrons (e_b) converted into hydrated electrons on top and half of this quantity on bottom.

be quantified; however, the concept of faradaic efficiency has to be invoked, which will be targeted in future work.

Last but not least, the effect of the term q_e in eq 14 on the hydrogen production is discussed based in the context of the results in Figure 7. Such a figure shows how the concentration of the major reactant evolves during the full period of discharge (0.2 ms) for the two extreme pHs. For pulsed DC-voltage from

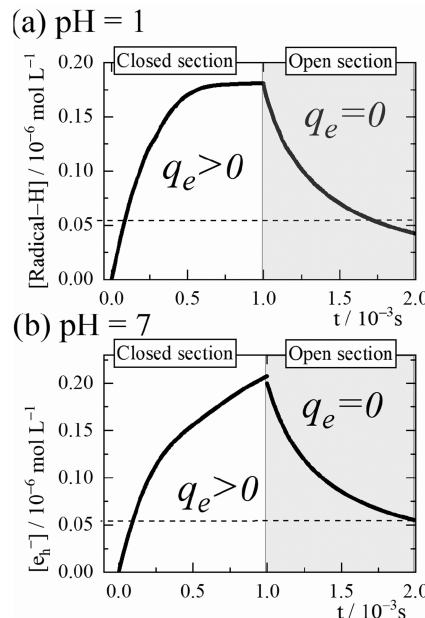


Figure 7. Temporal evolution for the major precursor of hydrogen at (a) pH = 1 and (b) pH = 7, accessed by computational experiments for solving eqs 21–23 as independent variables of the dynamical system. Initial conditions: [e_{aq}⁻]₀ = [•H]₀ = 10⁻¹⁷ M whereas [H⁺]₀ = [H⁺]_{bulk}. The values for all other parameters are listed in Table 1.

Urabe et al., the authors used a 50% duty cycle; therefore, the closed electrical circuit lasts 0.1 ms and another 0.1 ms is distributed at the opened circuit. On the basis of results from Figure 6, only 13% of the hydrogen yield is produced over an open circuit, while the other 87% is produced over a closed circuit, even though both sections had the same span time, 0.1 ms. Such a fact highlights the importance of the release rate of ballistic electrons (q_e) to accelerate the rates of reaction for the CNR proposed in Figure 2. In the closed section, the discharge itself closes the electrical circuit, a net electrical current flow throughout the plasma toward the liquid surface, and such a fact is connected to a fairly large positive value attributed to the term q_e . In the open section, opening the electrical circuit is observed and no net current flows throughout the electrical circuit, so, the term q_e acquires zero value. The implication of such time evolution of the plasma electrical variables connects to the temporal evolution for the concentration of the main reactants shown in Figure 7. Note that the radical-H is treated as a reactant because it is a key precursor of hydrogen at low pH. Under the closed section, the reactants only increase, whereas they only deplete under the open section. Engineering the duty cycle together with the current level seems to be a future direction to steer better energy efficiency for chemical synthesis, since decreasing the period under the closed section could bring advantages of saving input energy.

3.1.2. Air-Free Discharge over Alkaline Electrolyte (NaOH). In alkaline media, the initial concentration of H⁺ is rather low, between 10⁻⁷ and 10⁻¹⁴ mol L⁻¹. Such a low concentration of H⁺ slows down the rate of reactions 6, 7, and

8, thus via radical $\cdot\text{H}$ is seen to have a minor contribution over the total production of hydrogen. Figure 4 depicts this description for pH 7. For larger pH, such a contribution is even smaller as discussed in Figure 8, which shows the time profile

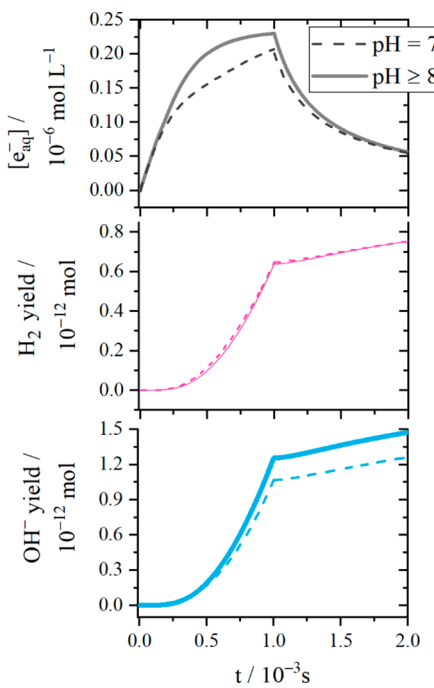


Figure 8. Effect of alkaline pH on the temporal evolution for the hydrated electron (top) along with the products such as hydrogen (center) and OH^- (bottom), accessed by computational experiments when solving eqs 21–23. Initial conditions: $[e_{aq}^-]_0 = [\cdot\text{H}]_0 = 10^{-17}\text{ M}$ whereas $[\text{H}^+]_0 = [\text{H}^+]_{\text{bulk}}$. The values for all other parameters are listed in Table 1.

for the concentration of the hydrated electron and for the yields of product considering neutral and alkaline pHs. This figure employs the dynamic system represented by eqs 21–23. At the extreme case of pH 8 and all larger values, the production of OH^- has been maximized. The inspection of ratio H_2 to OH^- shown in Figure 9 demonstrates that a ratio very close to 1:2 is found, indicating that the hydrated electrons pass to the unique reactant, and the self-recombination of hydrated electron is the main pathway for hydrogen production.

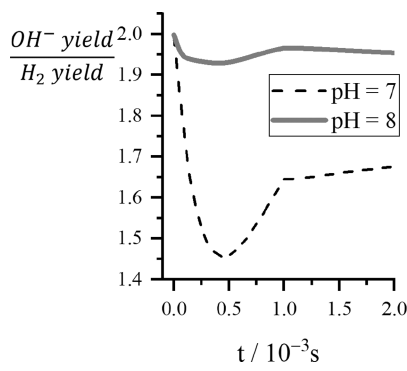


Figure 9. Effect of alkaline pH on the temporal evolution for ratio yield of OH^- to yields of hydrogen, when solving eqs 21–23 computationally.

Considering the CRN-tree in Figure 2, the unique relevant via in alkaline media with pH larger than 8 is the self-recombination of hydrated electron. Therefore, the eqs 22 and 23 from dynamic system represented by set of equations from eq 21 to eq 23 are eliminated because neither H^+ nor the $\cdot\text{H}$ are chemical variables. At pH larger than 8, the chemical dynamical system passes to be a subset of the CRN belonging to acid and neutral pH seen in the CRN-tree in Figure 2. The chemical dynamic model then is represented only by eq 27.

$$\frac{d[e_{aq}^-]}{dt} = -\{2k_1[e_{aq}^-]^2\} + \frac{1}{V}q_e \quad (27)$$

The products, or dependent variables, are represented by

$$\frac{d[\text{H}_2]}{dt} = k_1[e_{aq}^-]^2 \quad (28)$$

$$\frac{d[\text{OH}^-]}{dt} = 2k_1[e_{aq}^-]^2 \quad (29)$$

3.1.3. Air-Based Discharge over Neutral Electrolyte (NaCl).

This section is devoted to analyzing CRN in air-based discharge over a neutral electrolyte. For such boundary conditions, two chemical species take over the role of scavenger $S = \{\text{NO}_3^- \text{ and } \text{H}^+\}$ resulting in a CRN with three major reactants (NO_3^- , H^+ , and e_{aq}^-) and one intermediate species ($\cdot\text{H}$), as summarized by the CRN-tree in Figure 10. Additionally, the air-based discharge brings about two sources terms for scavengers $q_s \rightarrow q_{\text{H}^+}$ and $q_s \rightarrow q_{\text{NO}_3^-}$.

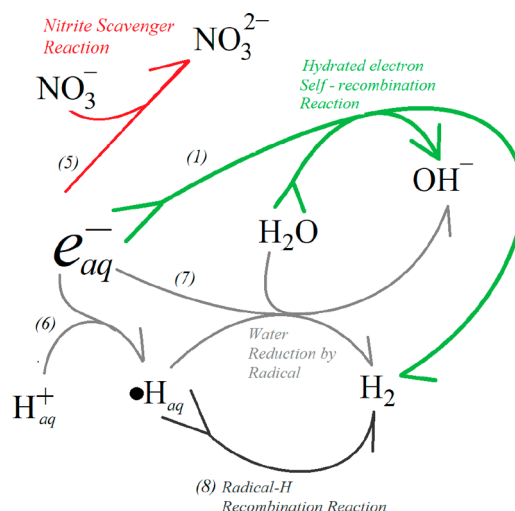


Figure 10. CRN-tree (or mechanism) for an air-based dry discharge over water containing NaCl as supporting electrolyte.

The temporal evolution of the reactants are accessed by

$$\begin{aligned} \frac{d[e_{aq}^-]}{dt} &= -\{2k_1[e_{aq}^-]^2 + k_6[\text{H}^+][e_{aq}^-] + k_7[\cdot\text{H}][e_{aq}^-]\} \\ &\quad + k_5[\text{NO}_3^-][e_{aq}^-] + \frac{1}{V}q_e \end{aligned} \quad (30)$$

$$\frac{d[\text{H}^+]}{dt} = -k_6[\text{H}^+][e_{aq}^-] + \frac{1}{V}q_{\text{H}^+} \quad (31)$$

$$\frac{d[\text{NO}_3^-]}{dt} = -k_5[\text{NO}_3^-][e_{aq}^-] + \frac{1}{V}q_{\text{NO}_3^-} \quad (32)$$

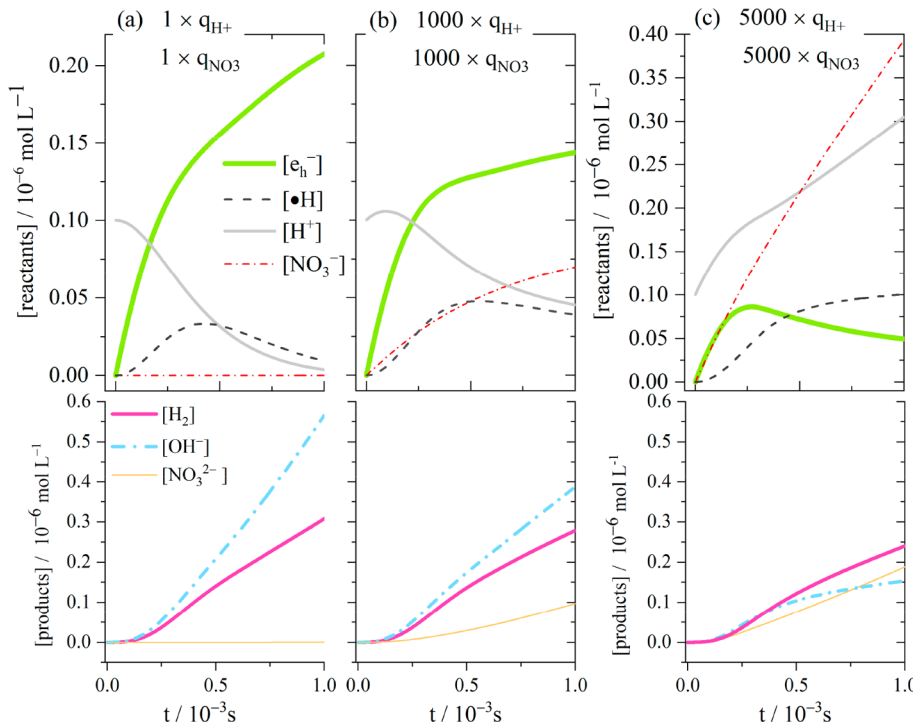


Figure 11. Temporal evolution of reactants (top) and products (bottom) accessed via interactive solution of the eqs 30–33 for initial concentrations of hydronium $[H^+]_0 = 10^{-7} \text{ mol L}^{-1}$ (for pH 7), but employing different values of the plasma-based source term $q = \{q_{H^+} \text{ and } q_{NO_3}\}$: (a) $q = 1 \times q$, (b) $q = 1000 \times q$, and (c) $q = 5000 \times q$. Initial condition: $[e_{aq}^-]_0 = [\bullet H]_0 = [NO_3^-]_0 = 10^{-17} \text{ M}$. The values for all other parameters are listed in Table 1.

Whereas the intermediate species (radical H^\bullet) is accessed by

$$\frac{d[H^\bullet]}{dt} = k_6[H^+][e_{aq}^-] - \{2k_8[\bullet H]^2 + k_7[\bullet H][e_{aq}^-]\} \quad (33)$$

And the products are accessed by

$$\frac{d[H_2]}{dt} = k_1[e_{aq}^-]^2 + k_8[\bullet H]^2 + k_7[\bullet H][e_{aq}^-] \quad (34)$$

$$\frac{d[OH^-]}{dt} = 2k_1[e_{aq}^-]^2 + k_7[\bullet H][e_{aq}^-] \quad (35)$$

$$\frac{d[NO_3^{2-}]}{dt} = k_5[NO_3^-][e_{aq}^-] \quad (36)$$

The air-based discharge over neutral electrolyte is an extension of the case studied in section 3.1.1. Figure 11 displays the results from numerical solution for a four-degree-of-freedom model that includes eqs 30–33 as the core dynamical system and eqs 34–36 as the dependent variables.

Interestingly, the presence of two plasma-induced sources of scavengers for the model from Figure 11, plate a, are insufficient to modify the final outcome when comparing to the findings from Figure 3, plate b. Both cases are solved for similar initial conditions except by a nonzero value for q_{H^+} and q_{NO_3} on Figure 11. The insignificance of the terms q_{H^+} and q_{NO_3} persists when conferring the yield of products from Figure 12 plate a and Figure 5 for pH 7. Such similarities indicates that the term $V^{-1} \times q_{NO_3}$ in eq 32 has a neglectful value in comparison to the term $k_5[NO_3^-][e_{aq}^-]$, which results in an invariable concentration of the nitrate as seen in Figure 11, plate a. Only if the value for q_{NO_3} , as seen in plates a–c, is

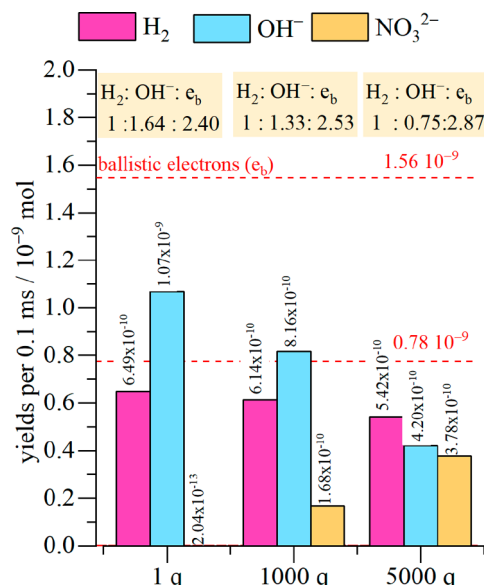
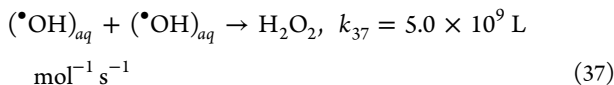


Figure 12. Yields of gaseous hydrogen, aqueous OH^- and NO_3^{2-} for pH 7 when solving eqs 30–33 by computational experiments for the period of closed section, i.e., 0.1 ms, and considering multiplied values for q_{NO_3} and q_{H^+} . Upper and bottom red dashed lines represent the values for full and half quantity of ballistic electrons (e_b) that had effectively crossed the plasma–liquid interface.

broadened in several folds, could a rise in the nitrate concentration be observed. Despite such enlargement on the source term q_{NO_3} impact on the yields of hydrogen, it is mild. Instead, the stoichiometry of OH^- and reduced nitrate (NO_3^{2-}) assumes an antagonist behavior, where the former

decreases whereas the latter enlarges; see Figure 12. Such antagonism reflects an interesting interference of the scavenger nitrate on the preferential route of hydrogen synthesis, favoring the route via radical-H in detriment of via-self. As the concentration of nitrate increases with enlarged q_{NO_3} , e_{aq}^- is further consumed by nitrate, decreasing concentration of e_{aq}^- that were what in fact determines a lesser hydrogen produced via-self (reaction 1). As were already mentioned on the discussion round Table 2, less OH^- is produced when accelerating the route of hydrogen synthesis via radical-H in detriment of the route via-self. Although on the switching preference on the routes, the yields of hydrogen is almost maintained, only decreasing in a stoichiometric content proportional to the decrease on the concentration of e_{aq}^- by the nitrate. Moreover, the minor impact of the nitrate concentration on the yields of hydrogen occurs because of the constrictions set for the model. It were settle that both sources q_{NO_3} and q_{H^+} acquired similar values because of the stoichiometry of reaction 20. The increasing value of source q_{H^+} guarantees a continuous supply of H^+ to the nanoreactor, which sustains an increased rate via radical-H with increased nitrate concentration, maintaining almost invariably the global production of hydrogen. The exclusion of air-based discharge from the list of drawbacks for hydrogen synthesis is an important point learned with this example.

3.2. Discharge in Humid Air over Oxygen-Free Electrolyte. This section devotes to understand the CRN for a discharge through humid noble gas. For a long time, it has been preconized that hydrogen peroxide is synthesized in the plasma phase⁴⁹ by water decomposition under discharge, followed afterward by its absorption onto the liquid surface. This understanding about the nature of the plasma–liquid interaction being restricted to an ordinary absorption of plasma precursor H_2O_2 by the liquid is reinforced in view of an enlarged yield of H_2O_2 when the contact area between plasma and liquid increases (achieved by flowing of water droplets through the plasma).⁵⁰ Other species such as radicals $\cdot\text{OH}$ and $\cdot\text{H}$ are also formed by the discharge under water vapor and their presence is also identified in liquid phase but via the spin-trapping technique.⁵ In view of everything said, H^+ , NO_3^- , and H_2O_2 , plus both radical $\cdot\text{OH}$ and $\cdot\text{H}$, represent the five scavengers considered as chemical variables for the CRN. However, H_2O_2 is excluded from this set of chemical variables, being treated instead as a dependent variable. Furthermore, this work adheres to the recent suggestion that only radical $\cdot\text{OH}$ is effectively solvated by the liquid, being H_2O_2 locally formed⁵¹ in the nanoreactor by reaction 37



According to this interpretation, all the locally formed H_2O_2 is transported through the liquid toward the bulk, which promotes its dissolution, in turn, weakening the scavenger-like action of reaction 4. For this reason, reaction 4 is fully disregarded in this approach. On the other hand, an enlarged concentration of $\cdot\text{OH}$ just strengthens its scavenger-like action via reaction 3. The present approach also tests the possible combination between $\cdot\text{OH}$ and $\cdot\text{H}$ by reaction 38

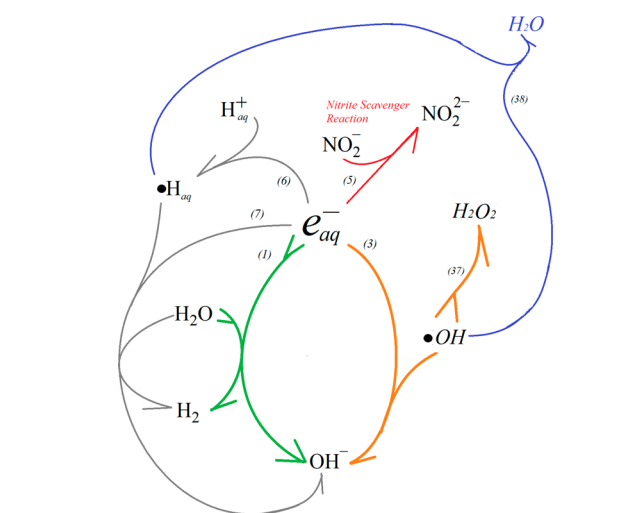
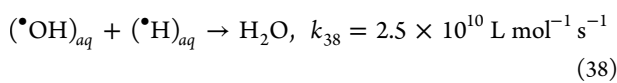


Figure 13. CRN-tree (or mechanism) for an air–based humid discharge over NaCl-containing water.

Figure 13 presents the CRN after all considerations mentioned above. The temporal evolution of the reactants in such CRN is accessed by

$$\frac{d[e_{aq}^-]}{dt} = -\{2k_1[e_{aq}^-]^2 + k_3[e_{aq}^-][\cdot\text{OH}] + k_5[e_{aq}^-][\text{NO}_3^-] + k_6[e_{aq}^-][\text{H}^+] + k_7[e_{aq}^-][\cdot\text{H}]\} + \frac{1}{V}q_e \quad (39)$$

$$\frac{d[\text{H}^+]}{dt} = -k_6[e_{aq}^-][\text{H}^+] + \frac{1}{V}q_{\text{H}^+} \quad (40)$$

$$\begin{aligned} \frac{d[\cdot\text{OH}]}{dt} = & -\{k_3[e_{aq}^-][\cdot\text{OH}] + k_{38}[\cdot\text{H}][\cdot\text{OH}] \\ & + 2k_{37}[\cdot\text{OH}]^2\} + \frac{1}{V}q_{\text{OH}} \end{aligned} \quad (41)$$

$$\frac{d[\text{NO}_3^-]}{dt} = -k_5[e_{aq}^-][\text{NO}_3^-] + \frac{1}{V}q_{\text{NO}_3} \quad (42)$$

Whereas the intermediate species (radical H^\bullet) is accessed by

$$\frac{d[\text{H}^\bullet]}{dt} = k_6[e_{aq}^-][\text{H}^+] - \{k_7[e_{aq}^-][\cdot\text{H}] + k_{38}[\cdot\text{H}][\cdot\text{OH}]\} \quad (43)$$

And the products are accessed by

$$\frac{d[\text{H}_2]}{dt} = k_1[e_{aq}^-]^2 + k_7[\text{H}^\bullet][e_{aq}^-] \quad (44)$$

$$\frac{d[\text{OH}^-]}{dt} = 2k_1[e_{aq}^-]^2 + k_3[e_{aq}^-][\cdot\text{OH}] + k_7[e_{aq}^-][\cdot\text{H}] \quad (45)$$

$$\frac{d[\text{NO}_3^{2-}]}{dt} = k_5[e_{aq}^-][\text{NO}_3^-], \quad (46)$$

$$\frac{d[\text{H}_2\text{O}_2]}{dt} = k_{37}[\cdot\text{OH}]^2 \quad (47)$$

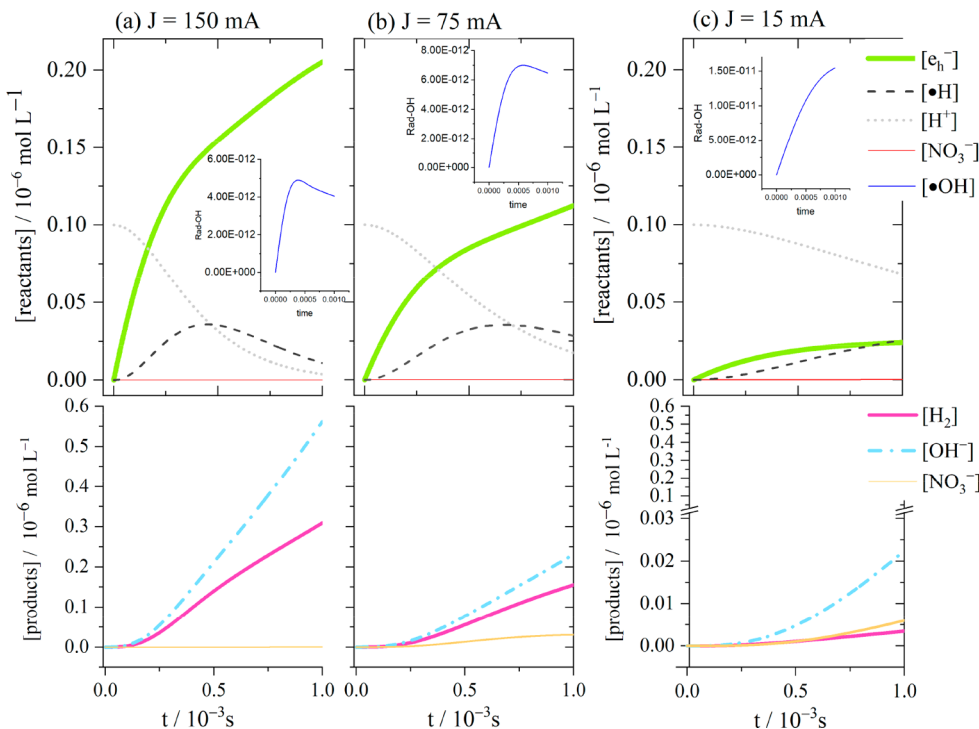


Figure 14. Temporal evolution of reactants and products accessed by computational experiments solving eqs 39–43 as independent variables of the dynamical system and considering three values for the level of current (a) 150, (b) 75, and (c) 15 mA. Initial conditions: $[e_{aq}^-]_0 = [\bullet H]_0 = 10^{-17} \text{ mol L}^{-1}$ whereas $[H^+]_0 = [H^+]_{\text{bulk}} = 10^{-7} \text{ mol L}^{-1}$. The values for all other parameters are listed in Table 1; a torch-like value was attributed to the term q_{OH^-} .

The five-degree-of-freedom model encompassed by the set of eqs 39–43 includes four source terms: q_e , q_{H^+} , $q_{NO_3^-}$, and q_{OH^-} . The values attributed to these source terms are found in Table 1. Detailed information about the estimations is found in Tables S3–S5, and the related discussion found in the Supporting Information. Figure 14 displays the results from numerical solution for eqs 39–43 (reactants) as the core dynamical system and eqs 44–47 (products) as the dependent variables.

Figure 14a displays results for discharge in gases containing water vapor that are commensurate with general trends already observed in Figure 11a for discharge in dry gases. Despite the fact that the mechanism in Figure 13 incorporates the radical OH as a chemical variable, the low value assigned to the term q_{OH^-} allows for such similarity. The plasma/liquid interaction for a torch-like discharge observed by Gorbanov et al.⁵ renders a term q_{OH^-} almost nine digits lower in the order of magnitude than a term q_{OH^-} estimated from the work of Lit et al.⁴⁶ for an anodic electrochemically discharged; cf. Table 1. Using the large term q_{OH^-} from anodic plasma is senseless in the context of this work because it analyses the chemical effects from a cathodic plasma. On the other hand, the electrical datum used in this work is among the largest current ever observed for a pulsed cathodic discharge, rendering the largest possible value attributed to source term of electrons (q_e). Conversely, for steady cathodic discharge,^{27,29} the current rarely exceeds 15 mA, rendering much lower values related to the term q_e . To cover the case of low current, some fractions of the current 150 mA are analyzed in Figure 14.

Respectively, a progressive and a sharp reduction on the generation of hydrogen is seen in Figure 14 when the current 150 mA is lowered by half in plate b and reduces to one tenth

in plate c. The tendencies of the temporal behaviors for the reactants in the plate b is maintained (i.e., a maximum on the radical-H profile, a substantial decay on the H^+ concentration, and a substantial increase on the e_{aq}^- concentration), meaning that reaction 1 still is the major route for e_{aq}^- consumption. Such conclusion agrees well with the minor variation on the stoichiometric proportion of products (ratio $H_2:OH^-:e_b$) seen in Figure 15, when comparing such a case (75 mA) to the 150 mA case. Furthermore, the larger deviation on the ballistic electron ratio upward of 2 for a current of 75 mA corroborates well with the fact that more e_{aq}^- had reacted with the nitrate, once the yield of reduced nitrate enlarges at 75 mA; cf. Figure 15. On the other hand, the current of 15 mA displays an out of proportionality reduction on the hydrogen yield, together with a change on the general tendency on the temporal evolution of reactants, strongly suggesting a change on the preferential route of the e_{aq}^- consumption. The rise on the radical-OH concentration is again very distinct from the other two larger currents whereas the concentration of radical-H and e_{aq}^- traces back each other. An assertive understanding on the preferential route of e_{aq}^- consumption could only be perceive if analyzing the rate of reactions as shown in Figure 16. An inversion on the dominant rate of reaction in relative terms is seen for the lowest current. Regarding the low current, Reaction 6 is the fastest one among all reactions in the CNR, leading to a substantial rise in the concentration of radical-H in the nanoreactor along the discharge. This happens because very little radical-H is consumed by the slow-rate reaction 7.

This section highlights the role of the current as a key parameter to modify the routes of e_{aq}^- consumption. As seen in this section, the scavenger-like action of the ion H^+ via reaction 6 is relevant only if in very low values of current.

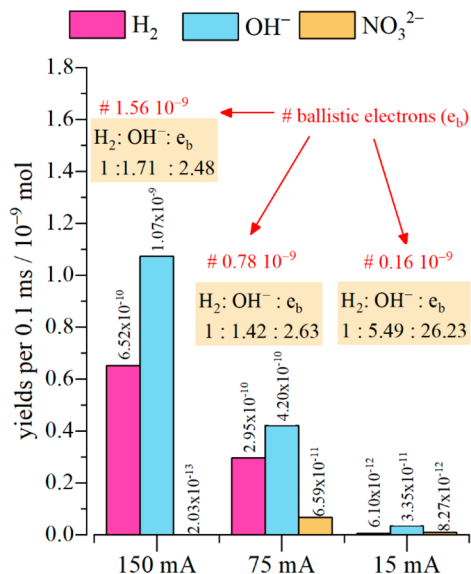


Figure 15. Yields of gaseous hydrogen, aqueous OH^- , and NO_3^{2-} when solving eqs 39–43 by computational experiments for the period of closed section, i.e., 0.1 ms, and considering multiplied values for the level of current, or alternatively, for the term q_e . The values of moles for the ballistic electrons (e_b) that had effectively crossed the plasma–liquid interface are indicated for each current.

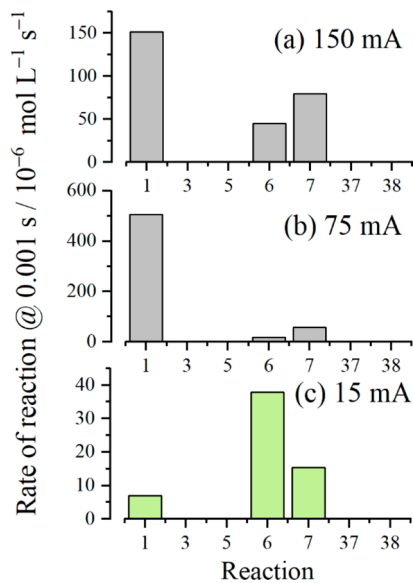


Figure 16. Rate of reactants accessed by computational experiments solving eqs 39–43 for the level of current (a) 150, (b) 75, and (c) 15 mA. Initial conditions: $[e_{aq}^-]_0 = [\bullet H]_0 = 10^{-17} \text{ mol L}^{-1}$ whereas $[H^+]_0 = [H^+]_{bulk} = 10^{-7} \text{ mol L}^{-1}$. The values for all other parameters are listed in Table 1; a torch-like value was attributed to the term q_{OH^-} .

3.3. Discharge in Humid Gas over Electrolyte Enriched with Dissolved Oxygen. This section envisions understanding the CRN for a discharge through humid air over a liquid body (aqueous electrolyte) that is enriched with soluble oxygen. It is well-known that liquid solubilizes gases throughout the gas–liquid interface; liquid water operates as solvent (or reservoir) for both oxygen and carbon dioxide. Taking into account the oxygen partial pressure in a humid air at sea level, 0.2095 atm, the concentration of oxygen is around $0.27 \times 10^{-3} \text{ mol L}^{-1}$, which is substantially high in comparison

to the e_{aq}^- concentration seen throughout this work. Conversely, the carbon dioxide has a very low partial pressure in air (0.0004 atm at sea level) that leads to concentration around $13 \times 10^{-6} \text{ mol L}^{-1}$, which is very more diluted than oxygen and could possibly scavenge e_{aq}^- in an extension relatively similar to the behavior found in Figure 3 for ions H^+ at pH 7. Given the high concentration of oxygen in water at sea level, this section considers the scavenger-like action solely for the dissolved oxygen.

The presence of soluble oxygen in aqueous phase introduces reaction 9–11 to the CNR previously considered in Figure 13. Besides this, reactions 38 and 5 are disregarded from this CNR. Reaction 5 effectively changes the distribution of products only if a source term q_{NO_3} is unrealistically high; thus, it is disregarded. Reaction 38 does play negligible roles for a high value of current (150 mA) since the distribution of products for this current at Figure 15 does adhere to stoichiometry related to a major domination of reaction 1; hence, this reaction 38 is eliminated. Taking all these considerations, the CNR proposed for the electrochemical discharge over an oxygen-enriched electrolyte for humid air-based gas phase is shown in Figure 17.

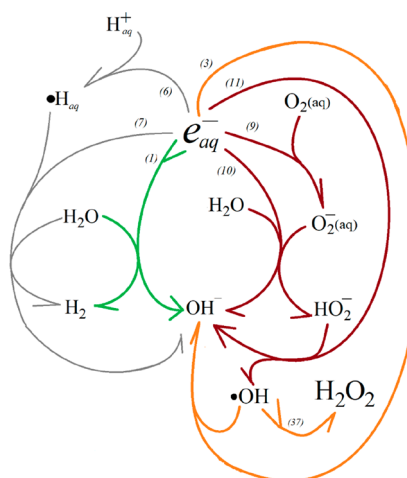


Figure 17. CRN-tree for air–free humid discharge over NaCl-containing water enriched with gaseous O_2 . For a less crowded graphical representation, water was cut out from the balance of reaction 11.

Temporal evolution of the reactants for the CNR in Figure 17 is accessed by

$$\begin{aligned} \frac{d[e_{aq}^-]}{dt} = & -\{2k_1[e_{aq}^-]^2 + k_3[e_{aq}^-][\bullet OH] + k_6[e_{aq}^-][H^+] \\ & + k_7[e_{aq}^-][\bullet H] + k_9[e_{aq}^-][O_2] + k_{10}[e_{aq}^-][O_2^-] \\ & + 2k_{11}[e_{aq}^-][HO_2^-]\} + \frac{1}{V}q_e \end{aligned} \quad (48)$$

$$\frac{d[H^+]}{dt} = -k_6[e_{aq}^-][H^+] \quad (49)$$

$$\begin{aligned} \frac{d[\bullet OH]}{dt} = & -\{k_3[e_{aq}^-][\bullet OH] + 2k_{37}[\bullet OH]^2\} \\ & + 2k_{11}[e_{aq}^-][HO_2^-] + \frac{1}{V}q_{OH} \end{aligned} \quad (50)$$

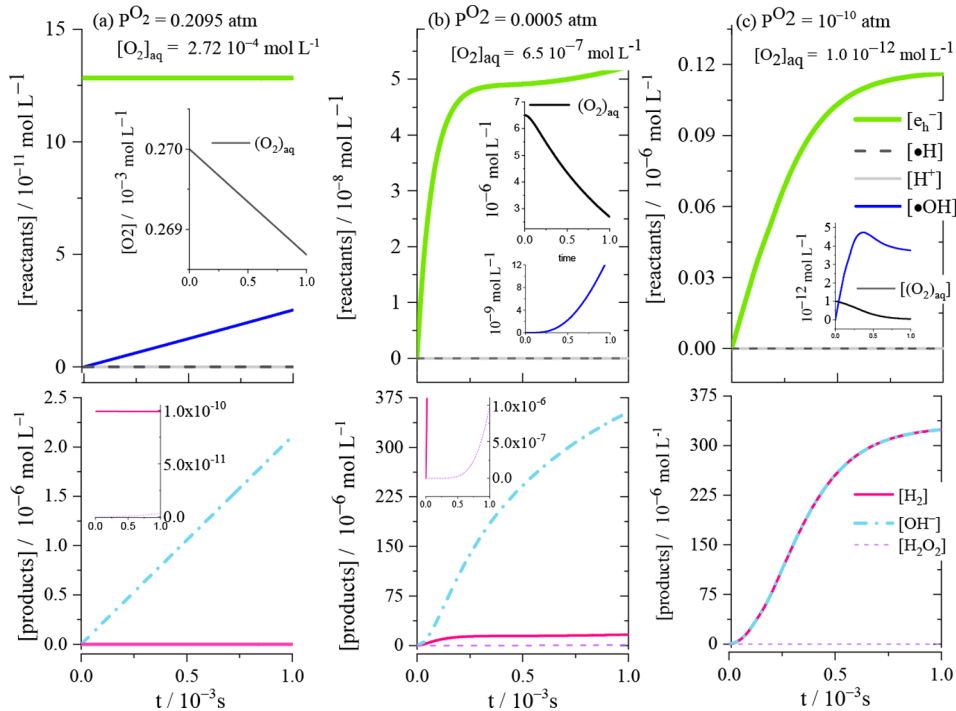


Figure 18. Temporal evolution of reactants and products accessed by computational experiments solving eqs 48–54 as independent variables of the dynamical system and considering three values for the level of current (a) 150, (b) 75, and (c) 15 mA. Initial conditions: $[e_{aq}^-]_0 = [\bullet H]_0 = 10^{-17}$ mol L⁻¹ whereas $[H^+]_0 = [H^+]_{bulk} = 10^{-7}$ mol L⁻¹. The values for all other parameters are listed in Table 1.

$$\frac{d[O_2]}{dt} = -k_9[e_{aq}^-][O_2] \quad (51)$$

Whereas the intermediate species is accessed by

$$\frac{d[H^\bullet]}{dt} = k_6[e_{aq}^-][H^+] - \{k_7[e_{aq}^-][\bullet H]\} \quad (52)$$

$$\frac{d[O_2^-]}{dt} = k_9[e_{aq}^-][O_2] - k_{10}[e_{aq}^-][O_2^-] \quad (53)$$

$$\frac{d[HO_2^-]}{dt} = k_{10}[e_{aq}^-][O_2^-] - 2k_{11}[e_{aq}^-][HO_2^-] \quad (54)$$

And the products are accessed by

$$\frac{d[H_2]}{dt} = k_1[e_{aq}^-]^2 + k_7[e_{aq}^-][\bullet H] \quad (55)$$

$$\begin{aligned} \frac{d[OH^-]}{dt} &= 2k_1[e_{aq}^-]^2 + k_3[e_{aq}^-][\bullet OH] + k_7[e_{aq}^-][\bullet H] \\ &+ k_{10}[e_{aq}^-][O_2^-] + 2k_{11}[e_{aq}^-][HO_2^-] \end{aligned} \quad (56)$$

$$\frac{d[H_2O_2]}{dt} = k_{37}[\bullet OH]^2 \quad (57)$$

Figure 18 shows the impact of partial pressure of oxygen (p^{O_2}) on the time evolution of reactants and products for the closed section of our model pulsed plasma. The oxygen concentration in the liquid is determined by the composition of the gas phase, measured in terms of p^{O_2} . The values attributed to the p^{O_2} correspond to the real life situations. For $p^{O_2} = 0.2019$ atm, air composes the gas phase. For $p^{O_2} = 0.0005$ atm, the gas phase is 99.95% of helium or argon, which corresponds to the real situation where the head of a closed chamber is filled with jet-plasma effluents as has been largely

employed by recent research using a electrochemical discharge. Finally, $p^{O_2} = 10^{-10}$ atm corresponds to an unrealistic experimental situation at atmospheric pressure, being more likely for unusual combinations of temperature and pressure. **Figure 18a** shows time evolution of reactants (top) and products (bottom) for 0.2095 atm p^{O_2} . It demonstrates that OH^- is the major final product and that the high oxygen concentration barely depletes during the discharge, indicating that oxygen scavengers all e_{aq}^- ; i.e., **reaction 9** majorly dominates the consumptions of e_{aq}^- . As the p^{O_2} decreases to 0.0005 atm, see panel b, the production of OH^- increases more than a hundred times whereas two significant changes happen to the reactant concentrations: the concentration of e_{aq}^- increases a thousand times and the initial concentration of oxygen is cut in half. Finally, for unusual 10^{-10} atm p^{O_2} , the scavenger-like action of aqueous oxygen has weakened because of its low concentration in liquid phase, enabling a substantial rise on the concentration of e_{aq}^- that follows up by a detectable production of hydrogen. However, as shown by the yields in **Figure 19**, this condition synthesizes hydrogen in a very inefficient way given that a large deviation on stoichiometric ratio $H_2: e_b$ is found, that is, the results display ratio equal 1:6 against 1:2 that is expected for one hundred efficiency of hydrates electrons consumptions toward hydrogen.

Beyond the distribution of products, the cases studied in this section also elucidates the dramatic impact of soluble oxygen on the spectrum of products. The neglectable production of both OH^- and H_2 seen for 0.2095 atm p^{O_2} in **Figure 19** indicates a change in the spectrum of final products. As **reaction 9** majorly dominates the consumptions of e_{aq}^- for 0.2095 atm p^{O_2} , the superoxide O_2^- is massively produced, an intermediate for the full mechanism but a product related to the **reaction 9**. The yields of superoxide O_2^- is account in **Figure 20**. Interestingly, its productions exhibits a ratio $H_2: e_b$

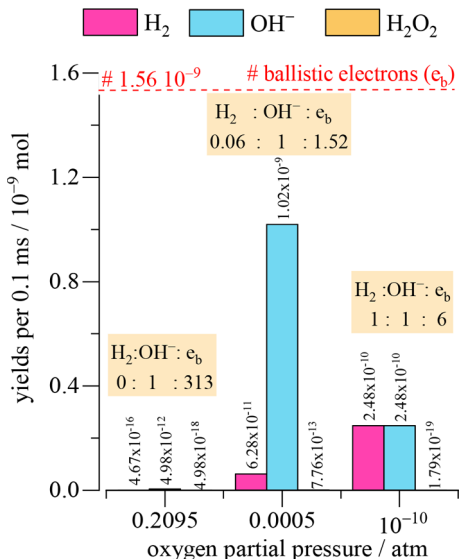


Figure 19. Yields of gaseous hydrogen, aqueous OH⁻, and hydrogen peroxide when solving eqs 48–54 by computational experiments for the period of closed section, i.e., 0.1 ms, and considering different values for the partial pressure of oxygen, which means alternatively to depart from the different initial concentrations of oxygen that is soluble in the aqueous phase.

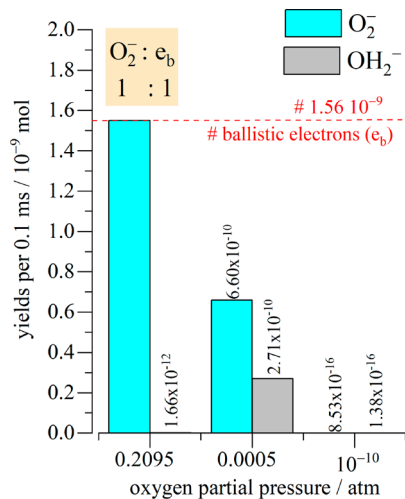


Figure 20. Yields of superoxide O²⁻ when solving eqs 48–54 by computational experiments for the period of closed section, i.e., 0.1 ms, and considering different values for the partial pressure of oxygen.

equals to 1:1 which does confirm that the hydrated electrons has been fully depleted toward superoxide O²⁻ for 0.2095 atm p_{O_2} . Such massive production of superoxide O²⁻ predicted in this work supports very much the recent findings of Shirai et al.⁵² The authors had detected superoxide O²⁻ in liquid phase for a electrochemical discharge whose gas/liquid interface exposes an large area for the gas/liquid surface at 0.2095 atm p_{O_2} .

4. DISCUSSION

Incontestably, experimental validation for the mechanism of hydrogen production proposed in this work depends on the simultaneous quantification of the stoichiometry proportion between H₂, OH⁻, and ballistic electrons (the number of ballistic electrons that effectively crossed the PLI, in turn,

converted into hydrated electrons). These three quantities (H₂:OH⁻:e_b) have to follow the stoichiometry 1:2:2, if hydrogen is majorly formed via self-recombination of hydrated electrons, as seen for the case of alkaline electrolyte (pH values above 8). If the electrolyte is strongly acid (pH around 1), those three quantities has to follow the stoichiometry 1:0:2, because hydrogen is majorly synthesized via radical-recombination reaction. For all the other cases in between these two extreme cases (i.e., 1 < pH < 8), the stoichiometric H₂:OH⁻:e_b tends to follow 1:x:2, where 0 < x < 2. Up to date, the experimental assessment to the stoichiometry H₂:OH⁻:e_b has been verified only partially. Using a salt as supporting electrolyte, so presumably at pH 7, Sengupta et al.⁴ have verified a stoichiometric ratio H₂:e_b equal to 1:1. cf. Figure 3 in ref 4 (findings that resembles the cathodic polarity). The results of Sengupta et al. strongly indicate that twice more hydrogen had been produced than expected by the chemical mechanism hereby proposed. Notoriously, some “water splitting” is developed on the plasma phase^{21,22,26} allowing for an excess of hydrogen production. Such plasma-induced radiolytic synthesis of hydrogen contributes to the global production of hydrogen under electrochemical discharge. Ultimately, experimental validation of the mechanism proposed in this work must circumvent plasma-phase radiolysis contribution; quenching of excited state water²³ could be a suitable strategy.

5. CONCLUSIONS

This paper deals with computational experiments employing chemical reactions networks (CRN) as a theoretical framework to explain events at the plasma–liquid interface for an electrochemical discharge, emphasizing the hydrogen synthesis as well as the drawbacks for its production. The generalist dynamic model for the plasma electrochemistry bases on the ordinary differential equations and includes a continuous function describing the chemical mechanism named function of the chemical reaction network (CRN). It also includes a source term (q), accounting for the plasma–liquid interaction, which could be of two natures, electrical (term q_e) and chemical (term q_s). Term q_e accounts for the injection of plasma-free electrons into the liquid, whereas term q_s accounts for the quantity of the species synthesized in the plasma phase that is absorption by the liquid. The physical boundary conditions enables one to solve the CRN-function for an infinitesimal volume containing approximately $\sim 10^{18}$ molecules of liquid water, termed a nanoreactor. The model is solved for different CRN via numerical methods.

The screening of CRN allows identification of two major pathways for gaseous hydrogen production. In strong acid media, ion H⁺ reacts with hydrated electrons forming radical-H (•H), an intermediate (and precursor) of gaseous hydrogen, whereas in strong alkaline media, the second-order recombination reaction of the hydrated electron predominantly yields the gaseous hydrogen. These paths are the “plasma version” of the hydrogen evolution ration (HER) observed on a standard solid/liquid interface for an electrochemical cathode. Any other side reaction consuming hydrated electrons competes with one of these two paths, decreasing the efficiency of hydrogen production.

Furthermore, this work identifies two disadvantageous experimental conditions for synthesizing hydrogen, which extends to other electrosynthesis routes. For a water-vapor-based discharge, the radical-OH produced in plasma-phase is

taken up by the liquid, decreasing yields of hydrogen in an extension very much dependent on the level of the electric current (term q_e in the model). However, the great villain against a large yield of hydrogen is the soluble oxygen. At room temperature and atmospheric pressure, the oxygen content in the air (around 0.21 atm of oxygen partial pressure) solubilizes into the liquid phase, resulting in a concentration very high in soluble oxygen. A massive production of superoxide O^{2-} and null production of hydrogen results from the complete consumption of the hydrated electrons by the aqueous oxygen. If, otherwise, 0.9995 atm of either He or Ar composes the gas phase (or 0.0005 atm of oxygen partial pressure), production of H_2 persists low. Tentatively, other techniques have to be used in association with low partial pressures of oxygen in order to circumvent the drawbacks related to the mass action of soluble oxygen in the liquid phase.

Finally, the computational experiments elucidates the interesting impact of the electrical current (or term q_e) and the rate of acidification (term q_s) on the hydrogen yields. These two terms, together, connect the properties of the plasma with the plasma-induced reactions in liquid phase, being the key parameters the developers of plasma source must target. At last, the assessment gained with the dynamical model, without loss of generality, can be extended to a set of reactions (or CNR-trees) for other routes of chemical synthesis in the emerging field of plasma electrochemistry.

■ ASSOCIATED CONTENT

Supporting Information

The Supporting Information is available free of charge on the ACS Publications website at DOI: [10.1021/acs.jpcc.9b04777](https://doi.org/10.1021/acs.jpcc.9b04777).

Glossary plus estimations on the parameters such as q_e and q_s , given in Tables S1–S5 ([PDF](#))

■ AUTHOR INFORMATION

Corresponding Author

*(A.M.-L.) E-mail: mota@usp.br.

ORCID

Andressa Mota-Lima: [0000-0002-6820-9797](https://orcid.org/0000-0002-6820-9797)

Author Contributions

The manuscript was written through contributions of all authors. All authors have given approval to the final version of the manuscript.

Notes

The authors declare no competing financial interest.

■ ACKNOWLEDGMENTS

This work was sponsored by CNPq (155046/2018-7). A.M.-L. is very much in debit to both Prof. Naoki Shirai and Prof. David Go for valuable discussions.

■ REFERENCES

- (1) Witzke, M.; Rumbach, P.; Go, D. B.; Sankaran, R M. Evidence for the electrolysis of water by atmospheric-pressure plasmas formed at the surface of aqueous solutions. *J. Phys. D: Appl. Phys.* **2012**, *45*, 442001.
- (2) Hickling, A.; Linacre, J. K. Glow-discharge electrolysis. Part II. The anodic oxidation of ferrous sulphate. *J. Chem. Soc.* **1954**, *711*–720.
- (3) Sen Gupta, S. K.; Singh, R. Cathodic contact glow discharge electrolysis: its origin and non-faradaic chemical effects. *Plasma Sources Sci. Technol.* **2017**, *26*, 015005.
- (4) Sengupta, S. K.; Singh, O. P. Contact glow discharge electrolysis: a study of its chemical yields in aqueous inert-type electrolytes. *J. Electroanal. Chem.* **1994**, *369*, 113–120.
- (5) Gorbanev, Y.; O'Connell, D.; Chechik, V. Non-Thermal Plasma in Contact with Water: The Origin of Species. *Chem. - Eur. J.* **2016**, *22*, 3496–3505.
- (6) Gorbanev, Y.; Stehling, N.; O'Connell, D.; Chechik, V. Reactions of nitroxide radicals in aqueous solutions exposed to non-thermal plasma: limitations of spin trapping of the plasma induced species. *Plasma Sources Sci. Technol.* **2016**, *25*, 055017–055027.
- (7) Tresp, H.; Hammer, M. U.; Winter, J.; Weltmann, K. D.; Reuter, S. Quantitative detection of plasma-generated radicals in liquids by electron paramagnetic resonance spectroscopy. *J. Phys. D: Appl. Phys.* **2013**, *46*, 435401–435409.
- (8) Sahni, M.; Locke, B. R. Quantification of Hydroxyl Radicals Produced in Aqueous Phase Pulsed Electrical Discharge Reactors. *Ind. Eng. Chem. Res.* **2006**, *45*, 5819–5825.
- (9) Lukes, P.; Locke, B. R. Plasmachemical oxidation processes in a hybrid gas–liquid electrical discharge reactor. *J. Phys. D: Appl. Phys.* **2005**, *38*, 4074–4081.
- (10) Delgado, H. E.; Radomsky, R. C.; Martin, D. C.; Bartels, D. M.; Rumbach, P.; Go, D. B. Effect of Competing Oxidizing Reactions and Transport Limitation on the Faradaic Efficiency in Plasma Electrolysis. *J. Electrochem. Soc.* **2019**, *166*, E181–E186.
- (11) Gorbanev, Y.; Leifert, D.; Studer, A.; O'Connell, D.; Chechik, V. Initiating radical reactions with non-thermal plasmas. *Chem. Commun.* **2017**, *53*, 3685–3688.
- (12) Snoeckx, R.; Wang, W.; Zhang, X.; Cha, M. S.; Bogaerts, A. Plasma-based multi-reforming for Gas-To-Liquid: tuning the plasma chemistry towards methanol. *Sci. Rep.* **2018**, *8*, 15929.
- (13) Barni, R.; Benocci, R.; Spinicchia, N.; et al. An Experimental Study of Plasma Cracking of Methane Using DBDs Aimed at Hydrogen Production. *Plasma Chem. Plasma Process.* **2019**, *39*, 241–259.
- (14) Barni, R.; Riccardi, C. Gas-phase evolution of Ar/H₂O and Ar/CH₄ dielectric barrier discharge plasmas. *Eur. Phys. J. D* **2018**, *72*, 62–71.
- (15) Yao, S. L.; Okumoto, M.; Nakayama, A.; Suzuki, E. Plasma Reforming and Coupling of Methane with Carbon Dioxide. *Energy Fuels* **2001**, *15*, 1295–1299.
- (16) Shapoval, V.; Marotta, E.; Ceretta, C.; Konjević, N.; Ivković, M.; Schirolin, M.; Paradisi, C. Development and Testing of a Self-Triggered Spark Reactor for Plasma Driven Dry Reforming of Methane. *Plasma Processes Polym.* **2014**, *11*, 787–797.
- (17) Wang, X.; Gao, Y.; Zhang, S.; Sun, H.; Li, J.; Shao, T. Nanosecond pulsed plasma assisted dry reforming of CH₄: The effect of plasma operating parameters. *Appl. Energy* **2019**, *243*, 132–144.
- (18) Huang, D.-Y.; Jang, J.-H.; Tsai, W.-R.; Wu, W.-Y. Improvement in Hydrogen Production with Plasma Reformer System. *Energy Procedia* **2016**, *88*, 505–509.
- (19) Mizeraczyk, J.; Jasinski, M. Plasma processing methods for hydrogen production*. *Eur. Phys. J.: Appl. Phys.* **2016**, *75*, 24702–24709.
- (20) Sengupta, S. K.; Singh, R.; Srivastava, A. K. A Study on the Origin of Nonfaradaic Behavior of Anodic Contact Glow Discharge Electrolysis: The Relationship Between Power Dissipated in Glow Discharges and Nonfaradaic Yields. *J. Electrochem. Soc.* **1998**, *145*, 2209–2213.
- (21) Janik, D.; Janik, I.; Bartels, D. M. Neutron and β/γ Radiolysis of Water up to Supercritical Conditions. 1. β/γ Yields for H₂, H• Atom, and Hydrated Electron. *J. Phys. Chem. A* **2007**, *111*, 7777–7786.
- (22) Schmidt, K. H.; Bartels, D. M. Lack of ionic strength effect in the recombination of hydrated electrons: $(e^-)_{aq} + (e^-)_{aq} \rightarrow 2(OH^-) + H_2$. *Chem. Phys.* **1995**, *190*, 145–152.
- (23) Horne, G. P.; Pimblott, S. M.; LaVerne, J. A. Inhibition of Radiolytic Molecular Hydrogen Formation by Quenching of Excited State Water. *J. Phys. Chem. B* **2017**, *121*, 5385–5390.
- (24) LaVerne, J. A.; Pimblott, S. M. New Mechanism for H₂ Formation in Water. *J. Phys. Chem. A* **2000**, *104*, 9820–9822.

- (25) Fourdrin, C.; Aarrachi, H.; Latrille, C.; Esnouf, S.; Bergaya, F.; Le Caér, S. Water Radiolysis in Exchanged-Montmorillonites: The H₂ Production Mechanisms. *Environ. Sci. Technol.* **2013**, *47*, 9530–9537.
- (26) Sterniczuk, M.; Bartels, D. M. Source of Molecular Hydrogen in High-Temperature Water Radiolysis. *J. Phys. Chem. A* **2016**, *120*, 200–209.
- (27) Rumbach, P.; Xu, R.; Go, D. B. Electrochemical Production of Oxalate and Formate from CO₂ by Solvated Electrons Produced Using an Atmospheric-Pressure Plasma. *J. Electrochem. Soc.* **2016**, *163*, F1157–F1161.
- (28) Kareem, T. A.; Kaliani, A. A. Glow discharge plasma electrolysis for nanoparticles synthesis. *Ionics* **2012**, *18*, 315–327.
- (29) Ghosh, S.; Hawtow, R.; Rumbach, P.; Go, D. B.; Akolkar, R.; Sankaran, R. M. Quantitative Study of Electrochemical Reduction of Ag⁺ to Ag Nanoparticles in Aqueous Solutions by a Plasma Cathode. *J. Electrochem. Soc.* **2017**, *164*, D818–D824.
- (30) Kondeti, V. S. S. K.; Gangal, U.; Yatom, S.; Bruggeman, P. J. Ag⁺ reduction and silver nanoparticle synthesis at the plasma–liquid interface by an RF driven atmospheric pressure plasma jet: Mechanisms and the effect of surfactant. *J. Vac. Sci. Technol., A* **2017**, *35*, 061302–061314.
- (31) Richmonds, C.; Witzke, M.; Bartling, B.; Lee, S. W.; Wainright, J.; Liu, C.-C.; Sankaran, R. M. Electron-Transfer Reactions at the Plasma–Liquid Interface. *J. Am. Chem. Soc.* **2011**, *133*, 17582–17585.
- (32) Maguire, P.; Rutherford, D.; Macias-Montero, M.; Mahony, C.; Kelsey, C.; Tweedie, M.; Pérez-Martin, F.; McQuaid, H.; Diver, D.; Mariotti, D. Continuous In-Flight Synthesis for On-Demand Delivery of Ligand-Free Colloidal Gold Nanoparticles. *Nano Lett.* **2017**, *17*, 1336–1343.
- (33) Patel, J.; Němcová, L.; Maguire, P.; Graham, W. G.; Mariotti, D. Synthesis of surfactant-free electrostatically stabilized gold nanoparticles by plasma-induced liquid chemistry. *Nanotechnology* **2013**, *24*, 245604.
- (34) Mariotti, D.; Patel, J.; Švrček, V.; Maguire, P. Plasma–Liquid Interactions at Atmospheric Pressure for Nanomaterials Synthesis and Surface Engineering. *Plasma Processes Polym.* **2012**, *9*, 1074–1085.
- (35) Shirai, N.; Uchida, S.; Tochikubo, F. Synthesis of metal nanoparticles by dual plasma electrolysis using atmospheric dc glow discharge in contact with liquid. *Jpn. J. Appl. Phys.* **2014**, *53*, 046202.
- (36) Gonçalves, I. A.; Barauna, J.; Cunha-Filho, F. J.; Chiavone-Filho, O.; Vitoriano, J. O.; Alves Júnior, C., Jr; Mota-Lima, A. Reduction of Aqueous Ag⁺ steered by electrochemical plasma: Connecting the Bulk pH Variation with the Reaction Pathways for Hydrated Electrons. *J. Braz. Chem. Soc.* **2019**, *30*, 1252–1265.
- (37) Rumbach, P.; Bartels, D. M.; Sankaran, R. M.; Go, D. B. The solvation of electrons by an atmospheric-pressure plasma. *Nat. Commun.* **2015**, *6*, 7248–7254.
- (38) Clarke, B. L. Stability of Complex Reaction Networks. *Advances in Chemical Physics* **1980**, *43*, 1–215.
- (39) Clarke, B. L. Complete set of steady states for the general stoichiometric dynamical system. *J. Chem. Phys.* **1981**, *75*, 4970–4979.
- (40) Eiswirth, M.; Freund, A.; Ross, J. Mechanistic Classification of Chemical Oscillators and the Role of Species. *Advances in Chemical Physics* **1991**, *80*, 127–199.
- (41) Garrett, B. C.; Dixon, D. A.; Camaioni, D. M.; Chipman, D. M.; Johnson, M. A.; Jonah, C. D.; Kimmel, G. A.; Miller, J. H.; Rescigno, T. N.; Rossky, P. J.; et al. Role of Water in Electron-Initiated Processes and Radical Chemistry: Issues and Scientific Advances. *Chem. Rev.* **2005**, *105*, 355–390.
- (42) Urabe, K.; Shirai, N.; Tomita, K.; Akiyama, T.; Murakami, T. Diagnostics of atmospheric-pressure pulsed-dc discharge with metal and liquid anodes by multiple laser-aided methods. *Plasma Sources Sci. Technol.* **2016**, *25*, 045004–045017.
- (43) Birkeland, K. On the oxidation of atmospheric nitrogen in electric arcs. *Trans. Faraday Soc.* **1906**, *2*, 98–116.
- (44) Rumbach, P.; Witzke, M.; Sankaran, R. M.; Go, D. B. Decoupling Interfacial Reactions between Plasmas and Liquids: Charge Transfer vs Plasma Neutral Reactions. *J. Am. Chem. Soc.* **2013**, *135*, 16264–16267.
- (45) Willis, C.; Boyd, A. W.; Rothwell, A. E.; Miller, O. A. Experimental and calculated yields in the radiolysis of water at very high dose rates. *Int. J. Radiat. Phys. Chem.* **1969**, *1*, 373–381.
- (46) Liu, J.; He, B.; Chen, Q.; Li, J.; Xiong, Q.; Yue, G.; Zhang, X.; Yang, S.; Liu, H.; Liu, Q. H. Direct synthesis of hydrogen peroxide from plasma-water interactions. *Sci. Rep.* **2016**, *6*, 38454.
- (47) Buxton, G. V.; Greenstock, C. L.; Helman, W. P.; Ross, A. B. Critical Review of rate constants for reactions of hydrated electrons, hydrogen atoms and hydroxyl radicals (·OH/·O⁻) in Aqueous Solution. *J. Phys. Chem. Ref. Data* **1988**, *17*, 513–886.
- (48) Lindsay, A.; Anderson, C.; Slikboer, E.; Shannon, S.; Graves, D. Momentum, heat, and neutral mass transport in convective atmospheric pressure plasma-liquid systems and implications for aqueous targets. *J. Phys. D: Appl. Phys.* **2015**, *48*, 424007.
- (49) Glasstone, S.; Hickling, A. 390. Studies in electrolytic oxidation. Part V. The formation of hydrogen peroxide by electrolysis with a glow-discharge anode. *J. Chem. Soc.* **1934**, 1772–1773.
- (50) Locke, B. R.; Shih, K.-Y. Review of the methods to form hydrogen peroxide in electrical discharge plasma with liquid water. *Plasma Sources Sci. Technol.* **2011**, *20*, 034006.
- (51) Rumbach, P.; Bartels, D. M.; Go, D. B. The penetration and concentration of solvated electrons and hydroxyl radicals at a plasma-liquid interface. *Plasma Sources Sci. Technol.* **2018**, *27*, 115013.
- (52) Shirai, N.; Suga, G.; Sasaki, K. Correlation between gas-phase OH density and intensity of luminol chemiluminescence in liquid interacting with atmospheric-pressure plasma. *J. Phys. D: Appl. Phys.* **2019**, *52*, 39LT02.